

Universality of many-body two-nucleon momentum distributions: the correlated nucleon spectral function of complex nuclei revisited

Claudio Ciofi degli Atti^{1*} and Hiko Morita^{2†}

¹*Istituto Nazionale di Fisica Nucleare, Sezione di Perugia,
c/o Department of Physics and Geology,*

University of Perugia, Via A. Pascoli, I-06123, Perugia, Italy

²*Sapporo Gakuin University, Bunkyo-dai 11, Ebetsu 069-8555, Hokkaido, Japan*

(Dated: March 12, 2022)

Background: The nuclear spectral function is a fundamental quantity which describes the mean-field and short-range correlation dynamics of nucleons embedded in the nuclear medium; its knowledge is a prerequisite for the interpretation of various electro-weak scattering processes off nuclear targets aimed at providing fundamental information on strong and weak interactions. Whereas in the case of the three-nucleon and, partly, the four-nucleon systems, the spectral function can be calculated *ab-initio* within a non-relativistic many-body Schroedinger approach, in the case of complex nuclei only models of the correlated, high momentum part of the spectral function are available so far.

Purpose: The purpose of this paper is to present a new approach such that the spectral function for a specific nucleus can be obtained from a reliable many-body calculation based upon realistic NN interactions, thus avoiding approximations leading to adjustable parameters.

Methods: The expectation value of the nuclear many-body Hamiltonian, containing realistic nucleon-nucleon interaction of the Argonne family, is evaluated variationally by a normalization conserving linked-cluster expansion and the resulting many-body correlated wave functions are used to calculate the one-nucleon and the two-nucleon momentum distributions; by analyzing the high momentum behavior of the latter, the spectral function can be expressed in terms of a transparent convolution formula involving the relative and center-of-mass (c.m.) momentum distributions in specific

regions of removal energy E and momentum k .

Results: It is found that as a consequence of the factorization of the many-body wave functions at short inter-nucleon separations, the high momentum behavior of the two-nucleon momentum distributions in $A = 3, 4, 12, 16, 40$ nuclei factorizes, at proper values of the relative and c.m. momenta, into the c.m. and relative momentum distributions, with the latter exhibiting a universal A -independent character. By exploiting the factorization property, it is found that the correlated part of the spectral function can be expressed in terms of a convolution formula depending upon the many-body relative and c.m. momentum distributions of a nucleon pair.

Conclusions: The obtained convolution spectral function of the three-nucleon systems, featuring both two-and three-nucleon short-range correlations, perfectly agrees in a wide range of momentum and removal energy with the *ab-initio* spectral function, whereas in the case of complex nuclei the integral of the obtained spectral functions (*the momentum sum rule*) reproduces with high accuracy the high momentum part of the one-nucleon momentum distribution, obtained independently from the Fourier transform of the non-diagonal one-body density matrix. Thus, the convolution spectral function we have obtained appears to indeed be a realistic microscopic, parameter-free quantity governed by the features of the underlying two-nucleon interactions.

PACS numbers: 25.30.Fj, 25.30.-c, 25.30.Rw, 21.90.+f

*Electronic address: ciofi@pg.infn.it

†Electronic address: hiko@webmail.sgu.ac.jp

I. INTRODUCTION: THE NUCLEON SPECTRAL FUNCTION

The hole spectral function (SF) of nucleon N_1 , $P_A^{N_1}(\mathbf{k}_1, E)$ is an important quantity playing a relevant role in the interpretation of various types of scattering processes off nuclei, in particular the electro-weak ones; as it is well known, it represents the joint probability that when nucleon “ N_1 ” (usually called the *active nucleon*) with momentum \mathbf{k}_1 is removed instantaneously from the ground state of the nucleus A , the nucleus $(A - 1)$ (usually called the *spectator nucleus*) is left in the excited state $E_{A-1}^* = E - E_{min}$, where E is the nucleon removal energy and $E_{min} = M_{A-1} + m_N - M_A = |E_A| - |E_{A-1}|$, with E_A and E_{A-1} being the (negative) ground-state energy of nuclei A and $A - 1$, respectively. The SF, which takes into account the fact that nucleons in nuclei have not only a momentum distribution, but also a distribution in energy, is trivially related to a well defined many-body quantity, namely the two-points Green’s function (see e.g. [1]). In what follows the well known representation of the SF will be used, namely

$$P_A^{N_1}(\mathbf{k}_1, E) = \frac{1}{2J+1} \sum_{M, \sigma_1} \langle \Psi_A^{JM} | a_{\mathbf{k}_1 \sigma_1}^\dagger \delta(E - (\hat{H}_A - E_A)) a_{\mathbf{k}_1 \sigma_1} | \Psi_A^{JM} \rangle \quad (1)$$

$$= \frac{1}{2J+1} \sum_{M, \sigma_1} \sum_f \left| \langle \Psi_{A-1}^f | a_{\mathbf{k}_1 \sigma_1} | \Psi_A^{JM} \rangle \right|^2 \delta(E - (E_{A-1}^f - E_A)) \quad (2)$$

$$= \frac{1}{2J+1} (2\pi)^{-3} \sum_{M, \sigma_1} \sum_f \left| \int d\mathbf{r}_1 e^{i\mathbf{k}_1 \cdot \mathbf{r}_1} G_f^{M\sigma_1}(\mathbf{r}_1) \right|^2 \delta(E - (E_{A-1}^f - E_A)), \quad (3)$$

where $a_{\mathbf{k}_1 \sigma_1}^\dagger$ ($a_{\mathbf{k}_1 \sigma_1}$) is the creation (annihilation) operator of a nucleon with momentum \mathbf{k}_1 and spin σ_1 , \hat{H}_A is the intrinsic Hamiltonian of A interacting nucleons, and the quantity

$$G_f^{M\sigma_1}(\mathbf{r}_1) = \langle \chi_{\sigma_1}^{1/2}, \Psi_{A-1}^f(\{\mathbf{x}\}_{A-1}) | \Psi_A^{JM}(\mathbf{r}_1, \{\mathbf{x}\}_{A-1}) \rangle, \quad (4)$$

which has been obtained by using the completeness relation for the eigenstates of the nucleus $(A - 1)$, $(\sum_f |\Psi_{A-1}^f\rangle \langle \Psi_{A-1}^f| = 1)$, is the overlap integral between the ground state wave function of nucleus A , Ψ_A^{JM} , and the wave functions of the discrete and all possible continuum eigenfunctions, Ψ_{A-1}^f (with eigenvalue $E_{A-1}^f = E_{A-1} + E_{A-1}^{f*}$), of nucleus $(A - 1)$; eventually, $\{\mathbf{x}\}$ denotes the set of spin-isospin and radial coordinates. The angle integrated SF is normalized according to

$$4\pi \int P_A^{N_1}(k_1, E) k_1^2 dk_1 dE = Z(N), \quad (5)$$

where $N(Z)$ denotes the number of proton (neutron) in the nucleus. The integral over the removal energy of the SF (the *momentum sum rule*) provides the one-nucleon momentum distribution

$$n_A^{N_1}(\mathbf{k}_1) = \int P_A^{N_1}(\mathbf{k}_1, E) dE, \quad (6)$$

which is linked to the two-nucleon momentum distribution $n_A^{N_1 N_2}(\mathbf{k}_1, \mathbf{k}_2)$, a quantity to be used in what follows, by the relation ($N_1 \neq N_2$)

$$n_A^{N_1}(\mathbf{k}_1) = \frac{1}{A-1} \left[\int n_A^{N_1 N_2}(\mathbf{k}_1, \mathbf{k}_2) d\mathbf{k}_2 + 2 \int n_A^{N_1 N_1}(\mathbf{k}_1, \mathbf{k}_2) d\mathbf{k}_2 \right]. \quad (7)$$

The one- and two-nucleon momentum distributions are defined as follows

$$n_A^{N_1}(\mathbf{k}_1) = \frac{1}{(2\pi)^3} \int d\mathbf{r}_1 d\mathbf{r}_1' e^{i\mathbf{k}_1 \cdot (\mathbf{r}_1 - \mathbf{r}_1')} \rho_A^{N_1}(\mathbf{r}_1; \mathbf{r}_1'), \quad (8)$$

and

$$n_A^{N_1 N_2}(\mathbf{k}_1, \mathbf{k}_2) = \frac{1}{(2\pi)^6} \int d\mathbf{r}_1 d\mathbf{r}_2 d\mathbf{r}_1' d\mathbf{r}_2' e^{i\mathbf{k}_1 \cdot (\mathbf{r}_1 - \mathbf{r}_1')} e^{i\mathbf{k}_2 \cdot (\mathbf{r}_2 - \mathbf{r}_2')} \rho_A^{N_1 N_2}(\mathbf{r}_1, \mathbf{r}_2; \mathbf{r}_1', \mathbf{r}_2'), \quad (9)$$

with the one- and two-nucleon non-diagonal density matrices, $\rho_A^{N_1}(\mathbf{r}_1; \mathbf{r}_1')$ and $\rho_A^{N_1 N_2}(\mathbf{r}_1, \mathbf{r}_2; \mathbf{r}_1', \mathbf{r}_2')$, being

$$\rho_A^{N_1}(\mathbf{r}_1; \mathbf{r}_1') = \int \psi_A^{JM*}(\mathbf{r}_1, \mathbf{r}_2, \mathbf{r}_3, \dots, \mathbf{r}_A) \hat{P}_{N_1}(1) \psi_A^{JM}(\mathbf{r}_1', \mathbf{r}_2, \mathbf{r}_3, \dots, \mathbf{r}_A) \delta\left(\sum_{i=1}^A \mathbf{r}_i\right) \prod_{i=2}^A d\mathbf{r}_i, \quad (10)$$

$$\begin{aligned} \rho_A^{N_1 N_2}(\mathbf{r}_1, \mathbf{r}_2; \mathbf{r}_1', \mathbf{r}_2') &= \int \psi_A^{JM*}(\mathbf{r}_1, \mathbf{r}_2, \mathbf{r}_3, \dots, \mathbf{r}_A) \hat{P}_{N_1}(1) \hat{P}_{N_2}(2) \psi_A^{JM}(\mathbf{r}_1', \mathbf{r}_2', \mathbf{r}_3, \dots, \mathbf{r}_A) \\ &\times \delta\left(\sum_{i=1}^A \mathbf{r}_i\right) \prod_{i=3}^A d\mathbf{r}_i, \end{aligned} \quad (11)$$

where $\hat{P}_N(i)$ is a projection operator on particle N . Unless differently stated, the following normalizations will be used in the rest of the paper

$$\int n_A^{N_1}(\mathbf{k}_1) d\mathbf{k}_1 = Z \Big|_{N_1=p} = N \Big|_{N_1=n}, \quad (12)$$

$$\int n_A^{N_1 N_2}(\mathbf{k}_1, \mathbf{k}_2) d\mathbf{k}_1 d\mathbf{k}_2 = \frac{Z(Z-1)}{2} \Big|_{N_1=N_2=p} = \frac{N(N-1)}{2} \Big|_{N_1=N_2=n} = ZN \Big|_{N_1=p, N_2=n} \quad (13)$$

with

$$\sum_{N_1 N_2} \int n_A^{N_1 N_2}(\mathbf{k}_1, \mathbf{k}_2) d\mathbf{k}_1 d\mathbf{k}_2 = \sum_{N_1 N_2} \int \rho_A^{N_1 N_2}(\mathbf{r}_1, \mathbf{r}_2) d\mathbf{r}_1 d\mathbf{r}_2 = \frac{A(A-1)}{2}. \quad (14)$$

It can be seen that the SF and the one- and two-nucleon momentum distributions have to satisfy simultaneously Eq. (6), and Eq. (7). However, whereas the calculation of the momentum distributions requires only the knowledge of the ground-state wave functions, the calculation of the SF requires the knowledge of both the ground-state wave function of nucleus A and the entire spectrum of wave functions of the nucleus $A - 1$. It is for this reason that the SF has been calculated exactly (*ab-initio*) only in the case of the three-nucleon systems (see [2] and [3]), and partly four-nucleon system [4], whereas in the case of complex nuclei only models can be produced. It should be stressed here, that one of the basic requirement for the validity of these models of the SF is the following: when they are integrated in the momentum sum rule (Eq. (6)), they have to provide the momentum distribution calculated independently by Eq.(8). If short-range correlations (SRC) are taken into account the angle-integrated nucleon SF is usually represented in the following form [5] ($|\mathbf{k}_1| \equiv k_1 \equiv k$)¹

$$P_A^{N_1}(k, E) = P_{MF}^{N_1}(k, E) + P_{SRC}^{N_1}(k, E), \quad (15)$$

with $P_{MF}^{N_1}$, describing the mean field (MF) structure of the nucleus, given by

$$P_{MF}^{N_1}(k, E) = \frac{1}{4\pi} \sum_{\alpha < \alpha_F} A_\alpha n_\alpha(k) \delta(E - |\epsilon_\alpha|), \quad (16)$$

where A_α denotes the number of particles in a pure low-momentum ($k \leq 1 - 1.5 \text{ fm}^{-1}$) shell-model state below the Fermi sea, characterized by a momentum distribution $n_\alpha(k)$ and spectroscopic factor

$$N_\alpha = \int_0^\infty n_\alpha^{SM}(k) k^2 dk < 1. \quad (17)$$

In momentum configuration, the first term in Eq. (15) describes the low momentum, partially occupied, ground-state shell-model components below the Fermi level, whereas the second term describes high momentum components created by SRC, whose main effect is to deplete the states below the Fermi level, creating occupied states above it. As already pointed out, the correlated part of the SF cannot be calculated exactly for $A > 4$; as a result, for complex nuclei essentially two models of the correlated SF have been developed

¹ Different but equivalent notations are used by different Authors e.g. $P^{N_1}(k, E) = P_0^{N_1}(k, E) + P_1^{N_1}(k, E)$, $P^{N_1}(k, E) = P_{gr}^{N_1}(k, E) + P_{ex}^{N_1}(k, E)$, and others.

so far. Both of them have the general structure of Eq. (15) and treat the uncorrelated part in the same way, but different models are used for the correlated part $P_{SRC}^{N_1}(k, E)$: in the first model [6] the calculated high momentum components in nuclear matter [7] are used for finite nuclei via the local density approximation (LDA), whereas in the second model [8] the high momentum components in the nuclear ground-state arise from a universal property of the ground-state wave function, namely its factorization into short-range and long-range parts in configuration space, arising whenever a pair of nucleons is located in the region of NN interaction dominated by SRC; in this case the SF is expressed in terms of quantities peculiar for the given nucleus, namely the center-of-mass (c.m.) and relative momentum distributions of a correlated nucleon pair. The first model has been intensively and successfully used in the description of electro-weak processes, in particular in neutrino scattering off nuclei (see e.g. [9]), whereas the second one was employed (see e.g. Ref.[10]) in the analysis of recent experimental data on SRC [11], in the interpretation of deep inelastic scattering [12] and in the extraction of the nucleon structure functions from DIS off nuclei [13]. The aim of the present paper is to illustrate a novel approach which extends the model of Ref. [8] leading to an improved realistic microscopic convolution model of the SF of complex nuclei.

II. FACTORIZATION OF THE MANY-BODY NUCLEAR WAVE FUNCTIONS AT SHORT RELATIVE DISTANCES AND THE CORRELATED MOMENTUM DISTRIBUTIONS

A. Factorization: the fundamental property of the nuclear wave function at short inter-nucleon ranges

The assumption of wave function factorization at short inter-nucleon ranges is a concept that has been frequently used in the past as a physically sound approximation of the unknown nuclear wave function, mainly to explain certain classes of medium-energy experiments (see e.g. [14]), without providing however any evidence of its quantitative validity, due to the lack, at that time, of realistic solutions of the nuclear many-body problem. These, however, became recently available and the validity of the factorization property could be checked. As a matter of fact, in the case of *ab initio* wave functions of few-nucleon systems [15] the factorization property of the wave functions has been demonstrated to hold, and the same

was shown to occur in the case of nuclear matter [16], treated within the Brueckner-Bethe-Goldstone (BBG) theory [17]; moreover, the general validity of the factorization property has also been demonstrated in several recent papers [18]. The first approach to employ factorization in order to obtain the SF appeared in Ref. [8]; there indeed it has been assumed that at short inter-nucleon relative distances $\mathbf{r}_{ij} = \mathbf{r}_i - \mathbf{r}_i$, much shorter than the center-of-mass coordinate $\mathbf{R}_{ij} = [\mathbf{r}_i + \mathbf{r}_i]/2$ the nuclear wave function

$$\Psi_A^{JM}(\{\mathbf{r}\}_A) = \hat{\mathcal{A}} \left\{ \sum_{n,m,f_{A-2}} a_{m,n,f_{A-2}} \left[\left[\Phi_n(\mathbf{x}_{ij}, \mathbf{r}_{ij}) \oplus \chi_m(\mathbf{R}_{ij}) \right] \oplus \Psi_{f_{A-2}}(\{\mathbf{x}\}_{A-2}, \{\mathbf{r}\}_{A-2}) \right] \right\} \quad (18)$$

can be written as follows (see also Ref. [18])²

$$\lim_{r_{ij} \ll R_{ij}} \Psi_A^{JM}(\{\mathbf{r}\}_A) \simeq \hat{\mathcal{A}} \left\{ \chi_{c.m.}(\mathbf{R}_{ij}) \sum_{n,f_{A-2}} a_{n,f_{A-2}} \left[\Phi_n(\mathbf{x}_{ij}, \mathbf{r}_{ij}) \oplus \Psi_{f_{A-2}}(\{\mathbf{x}\}_{A-2}, \{\mathbf{r}\}_{A-2}) \right] \right\}. \quad (19)$$

In Eqs. (18) and (19): i) $\{\mathbf{r}\}_A$ and $\{\mathbf{r}\}_{A-2}$ denote the set of radial coordinates of nuclei A and $A - 2$, respectively; (ii) \mathbf{r}_{ij} and \mathbf{R}_{ij} are the relative and c.m. coordinate of the nucleon pair ij , described, respectively, by a short-range relative wave function Φ_n and the c.m. wave function $\chi_{c.m.}$; iii) $\{\mathbf{x}\}_{A-2}$ and \mathbf{x}_{ij} denote the set of spin-isospin coordinates of the nucleus $(A - 2)$ and the pair (ij) . Placing Eq. (19) in the definition of the two-nucleon momentum distribution (Eq.(9)) and changing variables from $\mathbf{k}_1, \mathbf{k}_2$ to $\mathbf{k}_{rel} = (\mathbf{k}_1 - \mathbf{k}_2)/2$ and $\mathbf{K}_{c.m.} = \mathbf{k}_1 + \mathbf{k}_2$, the following expression of the two-nucleon momentum distributions is obtained in the region of factorization [19]

$$\begin{aligned} n_A^{N_1 N_2}(\mathbf{k}_1, \mathbf{k}_2) &= n_A^{N_1 N_2}(k_1, k_2, \theta_{12}) = n_A^{N_1 N_2}(k_{rel}, K_{c.m.}, \theta) \\ &\simeq n_{c.m.}^{N_1 N_2}(K_{cm}) n_{rel}^{N_1 N_2}(k_{rel}), \end{aligned} \quad (20)$$

which is the basic results underlying the short-range structure of nuclei, namely *at high values of $\mathbf{k}_{rel} \gg \mathbf{K}_{c.m.}$ ($\mathbf{r}_{rel} \ll \mathbf{R}_{c.m.}$) the momentum distribution of two correlated nucleons factorizes into the relative and c.m. momentum distributions, i.e. no longer depends upon angle θ between \mathbf{k}_{rel} and $\mathbf{K}_{c.m.}$.* In other words, when SRC are at work, the relative and c.m. motions are decoupled. A systematic analysis of factorization for nuclei with $A =$

² In Ref [8] it has been assumed that the c.m. of the pair moves in 0s state implying that factorization occurs only when the c.m momentum is very small ($K_{c.m.} \leq 1 \text{ fm}^{-1}$) with the high momenta being due only to the correlated pairs; as we shall see in what follows factorization can occur also when $K_{c.m.}$ is not necessary very low, provided $|\mathbf{k}_{rel}| \gg |\mathbf{K}_{c.m.}|$.

3, 4, 12, 16, 40 has been presented in Ref. [19] and the results of this paper allowed one to pick up the region of variation of the relative and c.m. momentum distributions where factorization takes place. This is a relevant achievement, for it allows us to obtain the SF in this region free of any adjustable parameter. Indeed the exact relation between one- and two-nucleon momentum distributions given by Eq. (7) can be expressed, *in the factorization region*, in terms of the following convolution formula ($\mathbf{k}_{rel} = [\mathbf{k}_1 - \mathbf{k}_2]/2 = \mathbf{k}_1 - \mathbf{K}_{c.m.}/2$)

$$n_A^{N_1}(\mathbf{k}_1) \simeq \left[\int n_{rel}^{N_1 N_2}(|\mathbf{k}_1 - \frac{\mathbf{K}_{c.m.}}{2}|) n_{c.m.}^{N_1 N_2}(\mathbf{K}_{c.m.}) d\mathbf{K}_{c.m.} + 2 \int n_{rel}^{N_1 N_1}(|\mathbf{k}_1 - \frac{\mathbf{K}_{c.m.}}{2}|) n_{c.m.}^{N_1 N_1}(\mathbf{K}_{c.m.}) d\mathbf{K}_{c.m.} \right] \equiv n_{SRC}^{N_1}(\mathbf{k}_1). \quad (21)$$

This represents the correlated momentum distributions which will be used in Section IV to obtain the correlated SF. Before that we will discuss in the next Section the situation concerning the feasibility of reliable many-body calculations based upon realistic models of the NN interaction, providing parameter-free ground-state wave functions which are necessary to produce the c.m. and relative momentum distributions.

III. MANY-BODY CALCULATIONS OF THE ONE-NUCLEON AND TWO-NUCLEON MOMENTUM DISTRIBUTIONS

A. The realistic many-body approach to the ground-state of nuclei

During the last few years the calculation of the ground-state property of few-nucleon systems and light nuclei (binding energy and radii, charge density and momentum distributions) has reached a high degree of sophistication so that quantities like Eqs. (8) and (9) can be calculated with ground-state wave functions $\Psi_A^{JM}(\{\mathbf{x}\})$ which are realistic solutions of the non-relativistic Schroedinger equation

$$\left[\sum_i \frac{\hat{\mathbf{p}}_i^2}{2m_N} + \sum_{i<j} \hat{v}_2(\mathbf{x}_i, \mathbf{x}_j) + \sum_{i<j<k} \hat{v}_3(\mathbf{x}_i, \mathbf{x}_j, \mathbf{x}_k) \right] \Psi_A^f(\{\mathbf{x}\}_A) = E_A^f \Psi_A^f(\{\mathbf{x}\}_A). \quad (22)$$

Here $\{\mathbf{x}\}_A \equiv \{\mathbf{x}_1, \mathbf{x}_2, \mathbf{x}_3, \dots, \mathbf{x}_A\}$ denotes the set of A generalized coordinates (the spatial coordinates satisfying the condition $\sum_{i=1}^A \mathbf{r}_i = 0$), f stands for the complete set of quantum numbers of state f and, eventually, \hat{v}_2 and \hat{v}_3 are realistic models of two-nucleon (2N) and

three-nucleon (3N) interactions. In what follows we will be mainly interested in the ground-state wave function $\Psi_A^{f=0} \equiv \Psi_0$. Once the interactions are fixed, Eq. (22) should be solved *ab initio*, i.e. exactly, which is possible only the case of few-nucleon systems with $A = 3, 4$; for $A > 4$ *ab initio* solutions cannot yet be found, and only approximate solutions, mostly based on the variational principle, are available. Eq. (22) has been solved within various many-body approaches using 2N interactions which explain two-nucleon bound and scattering data and, considering, also 3N interactions, which are introduced to explain the properties of the 3N bound states. In these calculations advanced forms of the NN interaction are provided by the so called Argonne family, in which case they have the following general form [20]

$$v(\mathbf{x}_i, \mathbf{x}_j) = \sum_{n=1}^{n_{max}} v^{(n)}(r_{ij}) \mathcal{O}_{ij}^{(n)}, \quad (23)$$

where $\mathbf{x}_k \equiv \{\mathbf{r}_k, \mathbf{s}_k, \mathbf{t}_k\}$ denotes the set of nucleon radial, spin and isospin coordinates, $\mathcal{O}_{ij}^{(n)}$ is a proper operator depending upon the orbital, spin and isospin momenta, and $n_{max} = 18$; in the case of purely central interaction one has $\mathcal{O}_{ij}^{(n=1)} = 1$ and $\mathcal{O}_{ij}^{(n>1)} = 0$, whereas in the realistic case the most important operators are as follows

$$\begin{aligned} \hat{\mathcal{O}}_{ij}^{(1)} &\equiv \hat{\mathcal{O}}_{ij}^c = 1 & \hat{\mathcal{O}}_{ij}^{(2)} &\equiv \hat{\mathcal{O}}_{ij}^\sigma = \boldsymbol{\sigma}_i \cdot \boldsymbol{\sigma}_j \\ \hat{\mathcal{O}}_{ij}^{(3)} &\equiv \hat{\mathcal{O}}_{ij}^\tau = \boldsymbol{\tau}_i \cdot \boldsymbol{\tau}_j & \hat{\mathcal{O}}_{ij}^{(4)} &\equiv \hat{\mathcal{O}}_{ij}^{\sigma\tau} = (\boldsymbol{\sigma}_i \cdot \boldsymbol{\sigma}_j) (\boldsymbol{\tau}_i \cdot \boldsymbol{\tau}_j) \\ \hat{\mathcal{O}}_{ij}^{(5)} &\equiv \hat{\mathcal{O}}_{ij}^t = \hat{S}_{ij} & \hat{\mathcal{O}}_{ij}^{(6)} &\equiv \hat{\mathcal{O}}_{ij}^{t\tau} = \hat{S}_{ij} (\boldsymbol{\tau}_i \cdot \boldsymbol{\tau}_j), \end{aligned} \quad (24)$$

where \hat{S}_{ij} is the tensor operator. Using such an NN potential, supplemented by 3N forces, *ab initio* solutions of the 3-body [21] and 4-body [22] nuclei, have been obtained. As for $A > 4$ nuclei realistic ground-state wave functions are available from variational calculations, i.e. from the minimization of the expectation value of realistic non relativistic Hamiltonians, namely

$$\langle \hat{H} \rangle = \frac{\langle \Psi_0 | \hat{H} | \Psi_0 \rangle}{\langle \Psi_0 | \Psi_0 \rangle} \equiv E_A^V \geq E_A^0, \quad (25)$$

assuming the following correlated wave function as the variational one

$$\Psi_0(\{\mathbf{x}\}_A) = \hat{F}(\{\mathbf{x}\}_A) \Phi_0(\{\mathbf{x}\}_A), \quad (26)$$

where $\Phi_0(\{\mathbf{x}\}_A)$ is a mean-field wave function and

$$\hat{F}(\{\mathbf{x}\}_A) = \hat{S}_A \prod_{i < j} \left[\sum_{n=1}^{n_{max}} f^{(n)}(r_{ij}) \hat{\mathcal{O}}_{ij}^{(n)} \right] \quad (27)$$

is a symmetrized (by the operator \hat{S}_A) product of operators $\hat{\mathcal{O}}_{ij}^{(n)}$ (the same that appear in the two-nucleon interaction (Eq. (23)) and $f^{(n)}$ is a correlation which reflects the features of the two-nucleon interaction and cures its possible singularities, e.g. if only central hard core interactions are considered, the well known Jastrow form is obtained [23]

$$\hat{F}_J(\{\mathbf{x}\}_A) = \prod_{i < j} f_C(r_{ij}), \quad (28)$$

where $f_C(r_{ij}) = 0$ when $r_{ij} \leq r_c$, if the two-nucleon potential exhibits a hard core of radius r_c . For complex nuclei with $A \leq 12$, Eq. (25) has been evaluated exactly within the Variational Monte Carlo (VMC) approach [24], based upon the numerical evaluation of the multidimensional integrals; by this way the VMC ground-state energy and wave-functions have been obtained and the momentum distributions were accordingly calculated. For $A > 12$ the increasing dimension of the required integrals related to the non central part of the potential, forbids till now the exact evaluation Eq. (25), so that some approximations are still necessary. In the Cluster Variational Monte Carlo (CVMC) [25] the contributions arising from the central part of the interaction are evaluated exactly with Jastrow-like wave functions, whereas the contributions arising from the non central part of the interaction were considered only for a limited number (five) of correlated nucleons; the CVMC has been recently applied to the description of ^{16}O and ^{40}Ca nuclei [26]. Thus due to the heavy numerical computation efforts required by the increasing number of nucleons, also CVMC is still difficult to perform and various alternative methods have been so far developed, based, in close analogy with the theory of quantum fluids [27], upon the evaluation of the leading contributions of Eq. (25); in particular, the following approaches should be mentioned: (i) the fermion hypernetted chain method (FHNC), where a certain class of contribution (the nodal diagrams), are summed to all orders (see: [28, 29]) and (ii) various cluster expansion approaches [30, 31] in which the expectation value of a given operator is rearranged in a series, whose zero-th order term is the mean field contribution and the n -th order term provides the contribution from n correlated nucleons. In this connection let us stress, as it is well known and also recently recalled [26], that the procedure of considering lowest order terms in the numerator and in the denominator of the expectation value of a certain operator and then taking their ratio, should not be pursued due to the presence, both in the numerator and the denominator, of unlinked terms which produce the divergence of the ratio with increasing number of particles. In our approach, we have followed the *normalization*

conserving linked cluster expansion (NCLCE) developed in Ref. [31], applied in the case of central interactions in Ref. [32] and generalized in Ref. [33] to the case of realistic interactions and applied to the calculations of the properties of ^{16}O and ^{40}Ca . The main feature of NCLCE can be illustrated in the simple case of the calculation of the expectation value of a generic operator $\hat{\mathcal{O}}$ and a Jastrow-like wave function, i. e. in the case of

$$\langle \hat{\mathcal{O}} \rangle = \frac{\langle \Psi | \hat{\mathcal{O}} | \Psi \rangle}{\langle \Psi | \Psi \rangle} = \frac{\langle \psi_{MF} | \prod f(r_{ij}) \hat{\mathcal{O}} \prod f(r_{ij}) | \psi_{MF} \rangle}{\langle \psi_{MF} | \prod f(r_{ij})^2 | \psi_{MF} \rangle}. \quad (29)$$

By writing

$$f(r_{ij})^2 = 1 + \eta(r_{ij}) \quad (30)$$

and expanding the resulting denominator in Eq. (29), $[1 + x]^{-1} = 1 - x + x^2 - \dots$, it can be shown that the unlinked terms in the numerator exactly cancel out the ones arising from the denominator and a convergent series expansion containing only linked terms is obtained in the following form

$$\langle \hat{\mathcal{O}} \rangle = \langle \psi_{MF} | \hat{\mathcal{O}} | \psi_{MF} \rangle + \langle \hat{\mathcal{O}} \rangle_1 + \langle \hat{\mathcal{O}} \rangle_2 + \dots + \langle \hat{\mathcal{O}} \rangle_n + \dots, \quad (31)$$

where the subscripts denote the number of η_{ij} appearing in the given term, $\langle \psi_{MF} | \hat{\mathcal{O}} | \psi_{MF} \rangle$ represents the MF uncorrelated contribution and the other terms represent the contribution from all linked and topologically distinct Iyon-Mayer diagrams [34], describing clusters of correlated nucleons³. For example the first order term is explicitly written as [33]

$$\begin{aligned} \langle \hat{\mathcal{O}} \rangle_1 &= \langle \psi_{MF} | \sum_{i < j} \left(f(r_{ij}) \hat{\mathcal{O}} f(r_{ij}) - \hat{\mathcal{O}} \right) | \psi_{MF} \rangle \\ &- \langle \psi_{MF} | \hat{\mathcal{O}} | \psi_{MF} \rangle \langle \psi_{MF} | \sum_{i < j} (f(r_{ij})^2 - 1) | \psi_{MF} \rangle. \end{aligned} \quad (32)$$

³ Note, in order to avoid confusions, that the first term of Eq. (31) is a pure independent-particle contribution, whereas in the definition of the SF (Eq. (15)) the mean-field part $P_{MF}^{N_1}(k, E)$ is renormalized by the spectroscopic factor of the single particle orbits.

If the correlation function has the form like Eq. (27), the above expression is extended to the following form

$$\begin{aligned} \langle \hat{\mathcal{O}} \rangle_1 &= \langle \psi_{MF} | \sum_{i < j} \left(\hat{f}(ij) \hat{\mathcal{O}} \hat{f}(ij) - \hat{\mathcal{O}} \right) | \psi_{MF} \rangle \\ &- \langle \psi_{MF} | \hat{\mathcal{O}} | \psi_{MF} \rangle \langle \psi_{MF} | \sum_{i < j} \left(\hat{f}(ij) \hat{f}(ij) - 1 \right) | \psi_{MF} \rangle, \end{aligned} \quad (33)$$

where

$$\hat{f}(ij) \equiv \sum_{n=1}^{n_{max}} f^{(n)}(\mathbf{r}_{ij}) \hat{\mathcal{O}}_{ij}^{(n)}. \quad (34)$$

The merit of this approach is the full cancelation of unlinked clusters contribution, which is a prerequisite for any convergent cluster expansion. The explicit expressions of the one- and two-nucleon non diagonal density matrices at the first order, which include up to clusters of four particles are given in Appendix. They are the basic quantities which are necessary to obtain the one-nucleon and two-nucleon momentum distributions.

Once the cluster expansion has been chosen the problem remains of the choice of the variational parameters which characterize both the wave function and the correlation functions. Indeed these have to be chosen as the ones which minimize the expectation value of the Hamiltonian (Eq. (25)). As far as the correlation functions are concerned, it is a common practice (see e.g. Ref. [29]) to obtain their shape by the minimization of the Hamiltonian at lowest order, obtaining by this way Euler-Lagrange equations which fix the shape of the correlation functions $f^{(n)}(r)$, according to the following conditions

$$f^{(p=1)}(r) = f_c(r) \rightarrow 1 \quad \text{at} \quad r \geq d \quad (35)$$

$$f^{(p>1)}(r) \rightarrow 0 \quad \text{as} \quad r \rightarrow \infty, \quad (36)$$

where d , the healing distance, representing the distance beyond which the two body correlated wave function $\psi(12)$ heals to the uncorrelated one $\phi(12)$, becomes the general variational parameter of the expansion together with the mean-field parameters. To sum up, there are at the moment realistic many-body wave functions, solutions of Eq. (22), which can be used to calculate realistic momentum distributions and model SF, without recurring to parameterized wave functions not corresponding to the minimization of the ground-state energy, or model wave functions containing adjustable parameters. At the same time, it turns out, as it will be shown in what follows, that the approach described above, namely a

parameter-free NCLCE can provide, with much less numerical efforts, results for the ground-state properties of light and medium weight nuclei in reasonable agreement with VMC [24] and CVMC results [26]. In the next Subsection, following Ref. [19], we will compare the results of our approach with the results of various many-body calculations of the ground-state energy and the one- and two-nucleon momentum distributions, whereas in Section IV, following the procedure of Ref. [35], we will present the results for the SF of complex nuclei.

B. Comparison of our results with the results of VMC and CVMC many-body approaches

1. Binding energies, two-nucleon correlation functions and one-nucleon momentum distribution

In Table I and Figs. 1-4 we compare the results of our NCLCE calculations with the results of other methods, particularly the VMC [24] and CVMC [26] ones obtained with similar NN interactions, omitting and including 3N forces. In Table I the values of the ground-state energy and r.m.s radii are compared, whereas Fig. 1 shows the two-body densities associated to the six correlation functions corresponding to the operators given in Eq. (24). An acceptable similarity of our results with the most advanced CVMC approach can be seen. In Fig. 2 we compare the one-nucleon momentum distribution of ^{16}O and ^{40}Ca we have obtained in Ref. [33] with recent CVMC results [26] and a remarkable agreement is evident ⁴. In Fig. 3 we also show the results of several different approaches to the momentum distributions of ^{16}O . Since, as usually, the momentum distributions are given on a log plot, in Fig.4 we show the quantity

$$\Delta n(k) = 100 \frac{n_x(k) - n_{\text{CVMC}}(k)}{n_{\text{CVMC}}(k)} \quad (37)$$

measuring the percent deviation of the theoretical momentum distribution of ^{16}O shown in Fig. 3, with respect to the CVMC results of Ref. [26], taken as the reference momentum distributions. From this plot it can again be seen that our one-nucleon momentum

⁴ In previous and present calculations we did not include the 3N interaction in Eq. (22), since we considered that the effects of the known 3N forces, conceived in order to provide the missing binding in ^3He , obtained when only 2N forces are considered, should not produce large effects on the high momentum content of the momentum distribution, as indeed was demonstrated by recent CVMC in ^{16}O and ^{40}Ca (see Figs. 11, 12 and 13 of Ref. [26])

distributions are sufficiently realistic ones.

2. Two-nucleon momentum distributions

In this subsection we will compare the two-nucleon momentum distributions calculated within the VMC approach [24] with the momentum distributions obtained within our NCLCE approach [19]. The two-nucleon momentum distribution is function of three variables, namely the relative momentum $|\mathbf{k}_{\text{rel}}| \equiv k_{\text{rel}}$, the c.m. momentum $|\mathbf{K}_{\text{c.m.}}| \equiv K_{\text{c.m.}}$ and the angle θ between them,

$$\begin{aligned} n_A^{N_1 N_2}(\mathbf{k}_{\text{rel}}, \mathbf{K}_{\text{c.m.}}) &= n_A^{N_1 N_2}(k_{\text{rel}}, K_{\text{c.m.}}, \theta) = \\ &= \frac{1}{(2\pi)^6} \int d\mathbf{r} d\mathbf{R} d\mathbf{r}' d\mathbf{R}' e^{i\mathbf{K}_{\text{c.m.}} \cdot (\mathbf{R} - \mathbf{R}')} e^{i\mathbf{k}_{\text{rel}} \cdot (\mathbf{r} - \mathbf{r}')} \rho_{N_1 N_2}^{(2)}(\mathbf{r}, \mathbf{R}; \mathbf{r}', \mathbf{R}'). \end{aligned} \quad (38)$$

Here we will consider two different momentum distributions namely: the c.m. momentum distribution

$$n_A^{N_1 N_2}(K_{\text{c.m.}}) = \int n_A^{N_1 N_2}(\mathbf{k}_{\text{rel}}, \mathbf{K}_{\text{c.m.}}) d\mathbf{k}_{\text{rel}} \equiv n_{\text{c.m.}}^{N_1 N_2}(K_{\text{c.m.}}), \quad (39)$$

shown in Fig. 5, and the relative momentum distribution

$$n_A^{N_1 N_2}(k_{\text{rel}}) = \int n_A^{N_1 N_2}(\mathbf{k}_{\text{rel}}, \mathbf{K}_{\text{c.m.}}) d\mathbf{K}_{\text{c.m.}}, \quad (40)$$

shown in Fig 6. It can be seen that an overall satisfactory agreement does indeed occurs between the VMC and the NCLCE approaches. The general θ -dependent two-nucleon momentum distribution (Eq. (38)) has already been presented in Ref. [19]. In this paper a new plot of this quantity will be given in the next Section.

3. Summary

An overall agreement of the results of calculations performed with VMC and NCLCE approaches has been found as far as the one-nucleon and two-nucleon relative and c.m momentum distributions of few-nucleon systems and medium-weight nuclei are concerned. Such an agreement makes us confident that the full momentum distributions calculated at different values of $K_{\text{c.m.}}$, k_{rel} and θ , the quantities which are necessary for the production of the nuclear SF, are genuine and realistic many-body quantities free of any adjustable parameter.

IV. WAVE FUNCTION FACTORIZATION AND THE MANY-BODY CONVOLUTION FORMULA OF THE CORRELATED SPECTRAL FUNCTION

A. The universal factorized behavior of the two-nucleon momentum distribution

In Section II we have demonstrated that if the two-nucleon momentum distribution factorize, the convolution formula of the SRC momentum distributions is obtained. By plotting the two-nucleon momentum distributions *vs* $|\mathbf{k}_{rel}|$ at different fixed values of the c.m. momentum $|\mathbf{K}_{c.m.}|$ and of the angle θ between the two momenta, it has indeed been shown [19] that at sufficiently high values of the relative momentum, such that $|\mathbf{k}_{rel}| \gg |\mathbf{K}_{c.m.}|$, the two-nucleon momentum distributions indeed factorize. In order to more quantitatively identify the factorization regions, in Fig. 7 we show a 3D plot of the two-nucleon momentum distribution pertaining to ${}^4\text{He}$ at $\theta = 0^\circ$ and $\theta = 90^\circ$ (similar results are available for other nuclei). The factorization regions, i.e. the region where the result at both angles coincide, can clearly be seen. A further important feature of factorization, which was overlooked in Ref. [19], but stressed in Ref. [35], is also visible: factorization is not only valid in the region of low c.m. momenta but also in the region of high c.m. momenta. In this respect it should be stressed that the minimum value of the relative momentum at which factorization starts to occur is a function of the value of the c.m. momentum $K_{c.m.}$, namely factorization is valid when

$$k_{rel} \gtrsim k_{rel}^-(K_{c.m.}), \quad (41)$$

with [35]

$$k_{rel}^-(K_{c.m.}) \simeq a + b \phi(K_{c.m.}), \quad (42)$$

where $a \simeq 1 \text{ fm}^{-1}$ and the function $\phi(K_{c.m.})$ is such that $\phi(0) \simeq 0$ ⁵. Since the value of k_{rel}^- depends upon the value of $K_{c.m.}$, Eq. (42) generates in Eq. (21) a constraint on the region of integration over $\mathbf{K}_{c.m.}$, in that only those values of $\mathbf{K}_{c.m.}$ satisfying Eq. (42) have to be

⁵ This condition is somewhat softer than that used for ${}^3\text{He}$ in Ref. [35]. Indeed we carefully reanalyzed the factorization-condition (Eq. (42)) and found that $k_{rel}^- = 1.0 + 0.5K_{c.m.}$ is the most accurate one within the linear- $K_{c.m.}$ dependence. Thus in the rest of the paper we use this factorization-condition also in the case of the ${}^3\text{He}$ SF.

considered. For a fixed value of k_1 the relation between k_1 and $K_{c.m.}$, given by

$$k_{rel} = |\mathbf{k}_1 - \frac{\mathbf{K}_{c.m.}}{2}| \geq k_{rel}^-(K_{c.m.}), \quad (43)$$

represents the equation which establishes a constraint on the the region of integration over $\mathbf{K}_{c.m.}$; this region becomes narrower than the region which is obtained if the constraint given by Eq. (43) is disregarded. It is worth stressing that except for Ref. [35], Eq. (43) and the resulting constraint were never been considered in the past.

The independence of the two-nucleon momentum distribution (Eq. (38)) upon the angle θ is direct proof that factorization does occur for both pn and pp SRC pairs, which means that

$$n_A^{N_1 N_2}(\mathbf{k}_1, \mathbf{k}_2) = n_A^{N_1 N_2}(k_{rel}, K_{c.m.}, \theta) \simeq n_{rel}^{N_1 N_2}(k_{rel}) n_{c.m.}^{N_1 N_2}(K_{c.m.}). \quad (44)$$

Moreover, in the case of pn pairs one finds [19]

$$n_A^{pn}(k_{rel}, K_{c.m.}) \simeq C_A^{pn} n_D(k_{rel}) n_{c.m.}^{pn}(K_{c.m.}); \quad (45)$$

where n_D is the deuteron momentum distribution and C_A^{pn} is a constant depending upon the atomic weight and which, together with the integrals of $n_D(k_{rel})$ and $n_{c.m.}^{pn}(K_{c.m.})$ in the proper SRC region, counts the number of SRC pn pairs in the given nucleus. Since the quantities $n_A^{pn}(k_{rel}, K_{c.m.})$, $n_D(k_{rel})$ and $n_{c.m.}^{pn}(K_{c.m.})$ are genuine many-body quantities, so is the value of C_A^{pn} given by

$$C_A^{pn} = \frac{n_A^{pn}(k_{rel}, K_{c.m.})}{n_D(k_{rel}) n_{c.m.}^{pn}(K_{c.m.})}. \quad (46)$$

Factorization, which has recently been confirmed also in Ref. [18], stays now on solid grounds, and so is the relation between the one-nucleon and two-nucleon momentum distributions given by Eq. (21). Whereas the pn two-nucleon momentum distribution in the factorization region can be expressed in terms of the deuteron momentum distribution, the pp distribution cannot be related to a known free pp function; nonetheless they also show a regularity which is exhibited for ^4He and ^{40}Ca in Figs. 8 and 9. These figures demonstrate that the k_{rel} dependence of the pp distribution at various values of $K_{c.m.}$ is governed in the factorization region by a common function of k_{rel} , with the amplitude determined by the value of $K_{c.m.}$. Thus if one defines the quantity

$$\tilde{n}_{rel}^{pp}(k_{rel}) = \frac{n_{rel}^{pp}(k_{rel}, K_{c.m.} = 0)}{n_{c.m.}(K_{c.m.} = 0)}, \quad (47)$$

one finds that in the factorization region the pp momentum distribution assumes the following form

$$n_A^{pp}(k_{rel}, K_{c.m.}) \simeq \tilde{n}_{rel}^{pp}(k_{rel}) n_{c.m.}(K_{c.m.}), \quad (48)$$

which exhibits, as clearly appears from Figs. 8 and 9, a very good agreement with the exact calculation.

We have now at disposal all microscopic many-body quantities to evaluate the one-nucleon SF, namely Eqs. (39), (45) and (48); having at disposal the SF we can calculate back the momentum distributions that, as previously stressed, has to coincide with the momentum distribution calculated directly with Eq.(8).

B. The spectral function of $A=3, 4, 12, 16, 40$

On the basis of what has been presented in the previous Sections, the total one-nucleon SF can be written in the following form

$$P_A^{N_1}(k, E) = P_{MF}^{N_1}(k, E) + P_{SRC}^{N_1}(k, E) \equiv P_{conv}(k, E) \quad (49)$$

where the mean-field contribution $P_{MF}^{N_1}(k, E)$ is given by Eq. (16) and

$$\begin{aligned} P_{SRC}^{N_1}(\mathbf{k}_1, E) &= \int n_{rel}^{N_1 N_2}(|\mathbf{k}_1 - \frac{\mathbf{K}_{c.m.}}{2}|) n_{c.m.}^{N_1 N_2}(\mathbf{K}_{c.m.}) d\mathbf{K}_{c.m.} \\ &\times \delta \left(E - E_{thr}^{N_1} - \frac{A-2}{2m_N(A-1)} \left[\mathbf{k}_1 - \frac{(A-1)\mathbf{K}_{c.m.}}{A-2} \right]^2 \right) \\ &+ 2 \int n_{rel}^{N_1 N_1}(|\mathbf{k}_1 - \frac{\mathbf{K}_{c.m.}}{2}|) n_{c.m.}^{N_1 N_1}(\mathbf{K}_{c.m.}) d\mathbf{K}_{c.m.} \\ &\times \delta \left(E - E_{thr}^{N_1} - \frac{A-2}{2m_N(A-1)} \left[\mathbf{k}_1 - \frac{(A-1)\mathbf{K}_{c.m.}}{A-2} \right]^2 \right) \end{aligned} \quad (50)$$

with $N_1 \neq N_2$. Let us remind that $P_{MF}^{N_1}(k, E)$ arises from the mean field, namely independent particle motion, whereas $P_{SRC}^{N_1}(\mathbf{k}_1, E)$ arises from the factorization of the nuclear wave function as in Eq. (19), assumed to hold (see also Ref. [8, 18]) when $\mathbf{r}_{ij} \ll \mathbf{R}$ (or $\mathbf{k}_{rel} \gg \mathbf{K}_{c.m.}$), the assumption that leads, in turns, to the factorization of the two-nucleon momentum and to Eq. (50).

Eq. (50) is the *convolution formula* of the correlated part of the SF. It represents the SF in the so-called plane wave approximation (PWA), which describes the process in which a correlated nucleon removed from a correlated pair, leaves the nucleus without interacting

with nucleus $A - 1$, whose excitation energy is therefore given by the sum of the threshold energy $E_{thr} = |E_A| - |E_{A-1}|$ plus the relative kinetic energy of the system: “*nucleus $(A - 2)$ -recoiling nucleon of the initially correlated pair*”. It has been shown in Ref. [35], on the example of the *ab-initio* 3N SF [3], that in a wide range of high values of momentum and removal energy typical of SRCs, the PWA SF is practically indistinguishable from the results of the Plane Wave Impulse Approximation (PWIA) SF in which the exact continuum two-nucleon wave function of the correlated pair is taken into account.

Let us now summarize two main features of the correlated SF:

- the correlated SF (50) depends upon two basic ground-state properties of nuclei, namely the c.m. and relative pn and pp momentum distributions, two quantities that have been calculated within advanced and rigorous many-body theories (VMC, NCLCE) so that Eq. (50) is a genuine realistic many-body quantity free of any adjustable parameter.
- the only model dependence of (50) resides in the argument of the energy-conserving delta function; such an approximation is justified by the high values of the removal energies characterizing the SRC SF;
- it should be stressed that Eq. (50) was essentially firstly obtained in Ref. [8] but applied there with phenomenological effective two-nucleon relative and c.m. momentum distributions. We should also point out that recently a model SF has been obtained within a relativistic kinematics approach [36], leading to the result of Ref. [8] in the non relativistic limit.

In Fig. 10 we show the proton and neutron SF of ^3He , calculated by Eq.(50), compared with the *ab-initio* SF of Ref. [3]; the SF of ^4He , ^{12}C , ^{16}O and ^{40}Ca , are shown in Fig. 11 where the separate contributions of pp and pn SRC are illustrated; the comparison with the convolution model of Ref. [8] is presented in Fig. 12. In all of these figure $k = 3.5 \text{ fm}^{-1}$. The k and E dependencies of the SF of Eq. (49) in the case of ^{12}C are shown in a 3D plot in Fig. 13. Let us comments the main features of these results. Concerning the three-nucleon system (see also Ref. [35]), it is very gratifying to observe a remarkable agreement of our convolution formula with the *ab initio* results in a wide range of removal energy, particularly in light of the absence of any adjustable parameter in Eq. (50); as for complex nuclei,

the small contribution of pp SRC with respect to pn SRC, in agreement with experimental evidences [11], should be stressed; concerning the differences between the present approach and the approach of Ref. [8], where the convolution formula for the SF has been firstly applied, the following remarks are in order:

1. both approaches have the same origin and structure, which is the convolution formula resulting from wave function factorization, with the main difference between the two approaches being related to the relative and c.m. momentum distributions used in the convolution formula; indeed in Ref. [8], due to the lack of realistic many-body calculations for complex nuclei, effective momentum distributions for pp and pn have been used, moreover at that time the region of factorization, which ensures the validity of the convolution formula, was unknown;
2. the differences between pp and pn momentum distributions, which is a prerequisite for extending the convolution approach to non-isoscalar asymmetric nuclei, have not been considered in Ref. [8], for the reasons given above;
3. in Ref. [8] only the soft part of the c.m. momentum distribution has been considered and the constraint on the values of $K_{c.m.}$ was disregarded.

In spite of these differences the two approaches seem to agree within about a 20 % accuracy.

As previously pointed out, any model for the SRC SF, when integrated over the removal energy in the momentum sum rule (Eq. (6)), has to provide the high momentum part of the one-nucleon momentum distribution obtained by the Fourier transform of the non-diagonal one-nucleon density matrix produced by the ground-state many-body wave functions. This is indeed the case of the convolution formula, as demonstrated in Fig. 14. Finally, in Fig. 15, the convergence of the momentum sum rule is shown: it can be seen that in order to correctly obtain the magnitude of the momentum distribution at $k \geq 4 \text{ fm}^{-1}$ the SF has to be integrated up to very high values of the removal energy ($E \simeq 400 \text{ MeV}$).

V. SUMMARY AND CONCLUSION

The main aspects and results of the present paper can be listed as follows:

1. the NCLCE was used to minimize the nuclear Hamiltonian of light nuclei containing realistic model of the nucleon-nucleon interaction and a comparison of the resulting

binding energies, radii, one- and two-nucleon momentum distributions, with particular emphasis on the high momentum components generated by SRC, have been calculated and shown to be in satisfactory agreement with the results of up-to-date approaches, like the VMC and CVMC ones;

2. we argued that the basis of any treatment of SRC is wave function factorization at short range and, accordingly, by a detailed analysis of the dependence of the two-nucleon momentum distribution $n_A^{N_1 N_2}(\mathbf{k}_{rel}, \mathbf{K}_{c.m.})$ upon the relative, \mathbf{k}_{rel} , and c.m., $\mathbf{K}_{c.m.}$, momenta of proton-neutron and proton-proton pairs embedded in the medium, we have demonstrated that in the region of momenta governed by the short-range behavior of the NN interaction ($|\mathbf{k}_{rel}| \geq 1 \text{ fm}^{-1}$, $|\mathbf{k}_{rel}| \gg |\mathbf{K}_{c.m.}|$) the two-nucleon momentum distributions factorize and the region of factorization of the nuclear wave function in momentum space has been clearly identified;
3. exploiting the factorization property of $n_A^{N_1 N_2}(\mathbf{k}_{rel}, \mathbf{K}_{c.m.})$ we have developed an advanced microscopic many-body, parameter-free approach to the SF which is expressed in terms of *ab-initio* A-dependent microscopic relative and c.m. momentum distributions, reflecting the underlying NN interaction; by this way, the specific features of a given nucleus are taken into account without recurring to any approximation;
4. in the case of the three-nucleon system, we found that the convolution formula fully agrees with the results of the *ab-initio* SF in a wide interval of momenta and removal energy;
5. in the case of complex nuclei the correctness of the convolution SF has been checked by means of the momentum sum rule, finding that the integral of the SF up to $E \simeq 400 \text{ MeV}$ fully agrees up to $k \simeq 5 \text{ fm}^{-1}$ with the exact one-nucleon momentum distribution, calculated independently in terms of the ground-state wave functions.

To summarize, we would like to stress that by exploiting the universal factorization property exhibited by the short-range behavior of the nuclear wave function for finite nuclei, we have generated a microscopic and parameter-free SF based upon a convolution of *ab initio* relative and c.m. two-nucleon momentum distributions for a given nucleus. The convolution SF rigorously satisfies the conditions for its validity, in that it takes into account only those nucleon configurations compatible with the requirement of wave function factorization. Our

convolution approach for the three-nucleon systems provides results in full agreement with proton and neutron SF, whereas in complex nuclei, for which *ab-initio* SF cannot yet be obtained, it fully satisfies the momentum sum rule. These results, coupled with the many-body microscopic nature of our approach and the absence of any adjustable parameter, makes the convolution SF a serious candidate for the investigation of nuclear effects in various processes, particularly in electro-weak scattering off nuclear targets. Needless to say that these processes besides a realistic SF, also require the inclusion of all types of final-state interaction which are at work when the active (struck) nucleon leaves the nucleus.

Appendix A: The one- and two-nucleon non diagonal density matrices with the NCLCE

1. One-nucleon non diagonal density matrix

The one-nucleon non diagonal density matrix at first order of the NCLCE includes three terms, namely:

$$\rho(\mathbf{r}_1, \mathbf{r}'_1) = \rho_{MF}(\mathbf{r}_1, \mathbf{r}'_1) + \rho_{2b}(\mathbf{r}_1, \mathbf{r}'_1) + \rho_{3b}(\mathbf{r}_1, \mathbf{r}'_1). \quad (\text{A1})$$

The suffixes (MF), (2b) and (3b) denote mean-field, 2-body and 3-body cluster term, respectively. Each term of Eq. (A1) is expressed by using the density distributions in mean-field given by

$$\rho_0(\mathbf{r}_i) = \sum_{n,l,m} |\varphi_{nlm}(\mathbf{r}_i)|^2, \quad \rho_0(\mathbf{r}_i, \mathbf{r}_j) = \sum_{n,l,m} \varphi_{nlm}^*(\mathbf{r}_i) \varphi_{nlm}(\mathbf{r}_j), \quad (\text{A2})$$

where we take the following mean-field wave function

$$\psi_{MF} = \frac{1}{\sqrt{A!}} \det[\phi_{\alpha_i}(x_j)], \quad \phi_{\alpha}(x_i) = \varphi_{nlm}(\mathbf{r}_i) \chi(i) \zeta(i), \quad (\text{A3})$$

with $\chi(i)$ and $\zeta(i)$ being the spin and isospin wave function respectively. The explicit form of each terms with the use of above quantities (Eq. (A2)) is shown what follows.

1.1 MF term

$$\rho_{SM}(\mathbf{r}_1, \mathbf{r}'_1) = 4\rho_0(\mathbf{r}_1, \mathbf{r}'_1). \quad (\text{A4})$$

1.2 2-body term

$$\begin{aligned} \rho_{2b}(\mathbf{r}_1, \mathbf{r}'_1) = \frac{1}{A} \int d\mathbf{r}_2 \quad & \left(< 12 | \hat{O}_{2b} | 12 >_{ST} \rho_0(\mathbf{r}_1, \mathbf{r}'_1) \rho_0(\mathbf{r}_2) \right. \\ & \left. - < 12 | \hat{O}_{2b} | 21 >_{ST} \rho_0(\mathbf{r}_1, \mathbf{r}_2) \rho_0(\mathbf{r}_2, \mathbf{r}'_1) \right), \end{aligned} \quad (\text{A5})$$

where following definitions for the matrix elements in the spin-isospin space are introduced

$$< ij | \hat{O}_{2b} | kl >_{ST} \equiv < \chi(i) \chi(j) \zeta(i) \zeta(j) | \hat{O}_{2b} | \chi(k) \chi(l) \zeta(k) \zeta(l) >, \quad (\text{A6})$$

$$\hat{O}_{2b} \equiv \hat{f}(12) \hat{f}(1'2) - 1.$$

1.3 3-body term

$$\rho_{3b}(\mathbf{r}_1, \mathbf{r}'_1) = \frac{1}{A} \int d\mathbf{r}_2 d\mathbf{r}_3 \rho_0(\mathbf{r}_1, \mathbf{r}_2) \quad (\text{A7})$$

$$\begin{aligned} & \times \left(< 123 | \hat{O}_{3b} | 231 >_{ST} \rho_0(\mathbf{r}_2, \mathbf{r}_3) \rho_0(\mathbf{r}_3, \mathbf{r}'_1) - < 123 | \hat{O}_{3b} | 213 >_{ST} \rho_0(\mathbf{r}_2, \mathbf{r}'_1) \rho_0(\mathbf{r}_3) \right), \\ \hat{O}_{3b} & \equiv \hat{f}(23) \hat{f}(23) - 1. \end{aligned} \quad (\text{A8})$$

2. Two-nucleon non diagonal density matrix

The two-nucleon non diagonal density matrix at first order of the NCLCE includes four terms, as follows

$$\begin{aligned} \rho^{pN}(\mathbf{r}_1, \mathbf{r}_2, \mathbf{r}'_1, \mathbf{r}'_2) &= \rho_{MF}^{pN}(\mathbf{r}_1, \mathbf{r}_2, \mathbf{r}'_1, \mathbf{r}'_2) + \rho_{2b}^{pN}(\mathbf{r}_1, \mathbf{r}_2, \mathbf{r}'_1, \mathbf{r}'_2) + \rho_{3b}^{pN}(\mathbf{r}_1, \mathbf{r}_2, \mathbf{r}'_1, \mathbf{r}'_2) \\ &+ \rho_{4b}^{pN}(\mathbf{r}_1, \mathbf{r}_2, \mathbf{r}'_1, \mathbf{r}'_2). \end{aligned} \quad (\text{A9})$$

The explicit forms of each term in Eq. (A9) are summarized what follows.

2.1 MF term

$$\rho_{MF}^{pn}(\mathbf{r}_1, \mathbf{r}_2, \mathbf{r}'_1, \mathbf{r}'_2) = \frac{1}{A(A-1)} 8\rho_0(\mathbf{r}_1, \mathbf{r}'_1)\rho_0(\mathbf{r}_2, \mathbf{r}'_2), \quad (\text{A10})$$

$$\rho_{MF}^{pp}(\mathbf{r}_1, \mathbf{r}_2, \mathbf{r}'_1, \mathbf{r}'_2) = \frac{2}{A(A-1)} (2\rho_0(\mathbf{r}_1, \mathbf{r}'_1)\rho_0(\mathbf{r}_2, \mathbf{r}'_2) - \rho_0(\mathbf{r}_1, \mathbf{r}'_2)\rho_0(\mathbf{r}_2, \mathbf{r}'_1)). \quad (\text{A11})$$

2.2 2-body term

$$\begin{aligned} \rho_{2b}^{pN}(\mathbf{r}_1, \mathbf{r}_2, \mathbf{r}'_1, \mathbf{r}'_2) &= \frac{1}{A(A-1)} \left(\langle 12|\hat{O}_{2b}|12 \rangle_{ST} \rho_0(\mathbf{r}_1, \mathbf{r}'_1)\rho_0(\mathbf{r}_2, \mathbf{r}'_2) \right. \\ &\quad \left. - \langle 12|\hat{O}_{2b}|21 \rangle_{ST} \rho_0(\mathbf{r}_1, \mathbf{r}_2)\rho_0(\mathbf{r}_2, \mathbf{r}'_1) \right), \end{aligned} \quad (\text{A12})$$

$$\hat{O}_{2b} \equiv \left(\hat{f}(12)\hat{f}(1'2') - 1 \right) \hat{P}^{pN}(12), \quad (\text{A13})$$

where $\hat{P}^{pN}(ij)$ is a projection operator on the pN pair.

2.2 3-body term

$$\rho_{3b}^{pN}(\mathbf{r}_1, \mathbf{r}_2, \mathbf{r}'_1, \mathbf{r}'_2) = \frac{2}{A(A-1)} \int d\mathbf{r}_3 F_{3b}^{pN}(\mathbf{r}_1, \mathbf{r}_2, \mathbf{r}'_1, \mathbf{r}'_2, \mathbf{r}_3), \quad (\text{A14})$$

$$F_{3b}^{pN} = \langle 123|\hat{O}_{3b}|123 \rangle_{ST} \rho_0(\mathbf{r}_1, \mathbf{r}'_1)\rho_0(\mathbf{r}_2, \mathbf{r}'_2)\rho_0(\mathbf{r}_3) \quad (\text{A15})$$

$$+ \langle 123|\hat{O}_{3b}|231 \rangle_{ST} \rho_0(\mathbf{r}_1, \mathbf{r}'_2)\rho_0(\mathbf{r}_2, \mathbf{r}_3)\rho_0(\mathbf{r}_3, \mathbf{r}'_1)$$

$$+ \langle 123|\hat{O}_{3b}|312 \rangle_{ST} \rho_0(\mathbf{r}_1, \mathbf{r}_3)\rho_0(\mathbf{r}_2, \mathbf{r}'_1)\rho_0(\mathbf{r}_3, \mathbf{r}'_2)$$

$$- \langle 123|\hat{O}_{3b}|132 \rangle_{ST} \rho_0(\mathbf{r}_1, \mathbf{r}'_1)\rho_0(\mathbf{r}_2, \mathbf{r}_3)\rho_0(\mathbf{r}_3, \mathbf{r}'_2)$$

$$- \langle 123|\hat{O}_{3b}|213 \rangle_{ST} \rho_0(\mathbf{r}_1, \mathbf{r}'_2)\rho_0(\mathbf{r}_2, \mathbf{r}'_1)\rho_0(\mathbf{r}_3)$$

$$- \langle 123|\hat{O}_{3b}|321 \rangle_{ST} \rho_0(\mathbf{r}_1, \mathbf{r}_3)\rho_0(\mathbf{r}_2, \mathbf{r}'_2)\rho_0(\mathbf{r}_3, \mathbf{r}'_1),$$

$$\hat{O}_{3b} \equiv \left(\hat{f}(13)\hat{f}(1'3) - 1 \right) \hat{P}^{pN}(12). \quad (\text{A16})$$

2.4 4-body term

$$\rho_{4b}^{pN}(\mathbf{r}_1, \mathbf{r}_2, \mathbf{r}'_1, \mathbf{r}'_2) = \frac{1}{2A(A-1)} \int d\mathbf{r}_3 d\mathbf{r}_4 F_{4b}^{pN}(\mathbf{r}_1, \mathbf{r}_2, \mathbf{r}'_1, \mathbf{r}'_2, \mathbf{r}_3, \mathbf{r}_4), \quad (\text{A17})$$

$$F_{4b}^{pN} = \langle 1234 | \hat{O}_{4b} | 2314 \rangle_{ST} (\rho_0(\mathbf{r}_1, \mathbf{r}'_2) \rho_0(\mathbf{r}_2, \mathbf{r}_3) \rho_0(\mathbf{r}_3, \mathbf{r}'_1) \rho_0(\mathbf{r}_4)) \quad (\text{A18})$$

$$\begin{aligned} & + \rho_0(\mathbf{r}_1, \mathbf{r}_2') \rho_0(\mathbf{r}_2, \mathbf{r}_4) \rho_0(\mathbf{r}_3) \rho_0(\mathbf{r}_4, \mathbf{r}_1') + \rho_0(\mathbf{r}_1, \mathbf{r}_3) \rho_0(\mathbf{r}_2, \mathbf{r}_1') \rho_0(\mathbf{r}_3, \mathbf{r}_2') \rho_0(\mathbf{r}_4) \\ & + \rho_0(\mathbf{r}_1, \mathbf{r}_4) \rho_0(\mathbf{r}_2, \mathbf{r}_1') \rho_0(\mathbf{r}_3) \rho_0(\mathbf{r}_4, \mathbf{r}_2') \\ & + \langle 1234 | \hat{O}_{4b} | 1342 \rangle_{ST} (\rho_0(\mathbf{r}_1, \mathbf{r}'_1) \rho_0(\mathbf{r}_2, \mathbf{r}_3) \rho_0(\mathbf{r}_3, \mathbf{r}_4) \rho_0(\mathbf{r}_4, \mathbf{r}'_2) \\ & + \rho_0(\mathbf{r}_1, \mathbf{r}'_1) \rho_0(\mathbf{r}_2, \mathbf{r}_4) \rho_0(\mathbf{r}_3, \mathbf{r}'_2) \rho_0(\mathbf{r}_4, \mathbf{r}_3) + \rho_0(\mathbf{r}_1, \mathbf{r}_3) \rho_0(\mathbf{r}_2, \mathbf{r}'_2) \rho_0(\mathbf{r}_3, \mathbf{r}_4) \rho_0(\mathbf{r}_4, \mathbf{r}'_1) \\ & + \rho_0(\mathbf{r}_1, \mathbf{r}_4) \rho_0(\mathbf{r}_2, \mathbf{r}'_2) \rho_0(\mathbf{r}_3, \mathbf{r}'_1) \rho_0(\mathbf{r}_4, \mathbf{r}_3)) \\ & + \langle 1234 | \hat{O}_{4b} | 3412 \rangle_{ST} (\rho_0(\mathbf{r}_1, \mathbf{r}_3) \rho_0(\mathbf{r}_2, \mathbf{r}_4) \rho_0(\mathbf{r}_3, \mathbf{r}'_1) \rho_0(\mathbf{r}_4, \mathbf{r}'_2) \\ & + \rho_0(\mathbf{r}_1, \mathbf{r}_4) \rho_0(\mathbf{r}_2, \mathbf{r}_3) \rho_0(\mathbf{r}_3, \mathbf{r}'_2) \rho_0(\mathbf{r}_4, \mathbf{r}'_1)) \\ & - \langle 1234 | \hat{O}_{4b} | 1324 \rangle_{ST} (\rho_0(\mathbf{r}_1, \mathbf{r}'_1) \rho_0(\mathbf{r}_2, \mathbf{r}_3) \rho_0(\mathbf{r}_3, \mathbf{r}'_2) \rho_0(\mathbf{r}_4) \\ & + \rho_0(\mathbf{r}_1, \mathbf{r}'_1) \rho_0(\mathbf{r}_2, \mathbf{r}_4) \rho_0(\mathbf{r}_3) \rho_0(\mathbf{r}_4, \mathbf{r}'_2) + \rho_0(\mathbf{r}_1, \mathbf{r}_3) \rho_0(\mathbf{r}_2, \mathbf{r}'_2) \rho_0(\mathbf{r}_3, \mathbf{r}'_1) \rho_0(\mathbf{r}_4) \\ & + \rho_0(\mathbf{r}_1, \mathbf{r}_4) \rho_0(\mathbf{r}_2, \mathbf{r}'_2) \rho_0(\mathbf{r}_3) \rho_0(\mathbf{r}_4, \mathbf{r}'_1)) \\ & - \langle 1234 | \hat{O}_{4b} | 2341 \rangle_{ST} (\rho_0(\mathbf{r}_1, \mathbf{r}'_2) \rho_0(\mathbf{r}_2, \mathbf{r}_3) \rho_0(\mathbf{r}_3, \mathbf{r}_4) \rho_0(\mathbf{r}_4, \mathbf{r}'_1) \\ & + \rho_0(\mathbf{r}_1, \mathbf{r}'_2) \rho_0(\mathbf{r}_2, \mathbf{r}_4) \rho_0(\mathbf{r}_3, \mathbf{r}'_1) \rho_0(\mathbf{r}_4, \mathbf{r}_3) + \rho_0(\mathbf{r}_1, \mathbf{r}_3) \rho_0(\mathbf{r}_2, \mathbf{r}'_1) \rho_0(\mathbf{r}_3, \mathbf{r}_4) \rho_0(\mathbf{r}_4, \mathbf{r}'_2) \\ & + \rho_0(\mathbf{r}_1, \mathbf{r}_4) \rho_0(\mathbf{r}_2, \mathbf{r}'_1) \rho_0(\mathbf{r}_3, \mathbf{r}'_2) \rho_0(\mathbf{r}_4, \mathbf{r}_3)) \\ & - \langle 1234 | \hat{O}_{4b} | 3421 \rangle_{ST} (\rho_0(\mathbf{r}_1, \mathbf{r}_3) \rho_0(\mathbf{r}_2, \mathbf{r}_4) \rho_0(\mathbf{r}_3, \mathbf{r}'_2) \rho_0(\mathbf{r}_4, \mathbf{r}'_1) \\ & + \rho_0(\mathbf{r}_1, \mathbf{r}_4) \rho_0(\mathbf{r}_2, \mathbf{r}_3) \rho_0(\mathbf{r}_3, \mathbf{r}'_1) \rho_0(\mathbf{r}_4, \mathbf{r}'_2)), \end{aligned}$$

$$\hat{O}_{4b} \equiv \left(\hat{f}(34) \hat{f}(34) - 1 \right) \hat{P}^{pN}(12). \quad (\text{A19})$$

-
- [1] W. H. Dickoff, D. V. van Neck, *Many-Body Theory Exposed*, World Scientific, 2010.
 - [2] A. E. L. Dieperink, T. de Forest, Jr., I. Sick, R. A. Brandenburg, Phys. Lett. **63B**, 261 (1976).
C. Ciofi degli Atti, E. Pace, G. Salmè, Phys. Rev. **C21**, 805 (1980).
H. Meier-Hajduk, Ch. Hajduk, P. E. Sauer, W. Thies, Nucl. Phys. **A395**, 332 (1983).
A. Kievsky, E. Pace, G. Salmè, M. Viviani, Phys. Rev. Cbf **56**, 64 (1997).
 - [3] C. Ciofi degli Atti, L. P. Kaptari Phys. Rev. **C71**, 024005 (2005).
 - [4] H. Morita, T. Suzuki, Progr. Theor. Phys. **86**, 671 (1991)
 - [5] C. Ciofi degli Atti, S. Liuti, S. Simula, Phys. Rev. **C41**, R2474 (1990).
 - [6] O. Benhar, A. Fabrocini, S. Fantoni, I. Sick Nucl. Phys. **A579**, 493 (1994).
 - [7] O. Benhar, A. Fabrocini, S. Fantoni, G. A. Miller, V. R. Pandharipande, I. Sick, Phys. Rev. **44**, 2328 (1991).
 - [8] C. Ciofi degli Atti and S. Simula, Phys. Rev. **C53**, 1689 (1996).
 - [9] O. Benhar, N. Farina, H. Nakamura, M. Sakuda, R. Seki, Phys. Rev. **D72**, 053005 (2005).
 - [10] C. Ciofi degli Atti, Phys. Rept. **590**, 1 (2015).
 - [11] O. Hen, G. A. Miller, E. Piasetzky, L. B. Weinstein, Rev. Mod. Phys. (to appear) (arXiv:1611.09748v4 [nucl-ex] 13 Apr 2017)
O. Hen et al.(CLAS Collaboration) Science **346**, 614 (2014); (arXiv:1412.0138 [nucl-ex])
 - [12] C. Ciofi degli Atti, S. Liuti, Phys. Lett. **B225**, 215 (1989).
C. Ciofi degli Atti, L. Frankfurt, L. P. Kaptari, M. I. Strikman, Phys. Rev. **C76**, 055206 (2007).
O. Hen, D. W. Higinbotham, G. A. Miller, E. Piasetzky, L. B. Weinstein, Int. Jour. Mod. Phys. **E22**, 1330017(2017).
 - [13] S. A. Kulagin, R. Petti, Nucl. Phys. **A765**, 126 (2006).
 - [14] J. S. Levinger, Phys. Rev. **84**, 43 (1951).
 - [15] C. Ciofi degli Atti, L. P. Kaptari, S. Scopetta and H. Morita, Few Body Syst. **50**, 243 (2011).
 - [16] M. Baldo, M. Borromeo and C. Ciofi degli Atti, Nucl. Phys. A **604**, 429 (1996).
 - [17] B. D. Day, Rev. Mod. Phys. **50**, 495 (1978).
 - [18] R. Weiss, B. Bazak, N. Barnea, Phys. Rev. Lett. **114**, 012501 (2015).

- R. Weiss, B. Bazak and N. Barnea, Phys. Rev. C**92**, 054311 (2015).
- R. Weiss, B. Bazak, N. Barnea, Eur.Phys.Jour. A**52**, 92(2016).
- R. Weiss, R. Cruz-Torres, N. Barnea, E. Piasetzky and O. Hen, arXiv:1612.00923v1 [nucl-th] (2016).
- [19] M. Alvioli, C. Ciofi degli Atti, H. Morita, Phys. Rev. C**94**, 044309 (2016).
- M. Alvioli, C. Ciofi degli Atti and H. Morita, Phys. Rev. Lett. **100**, 162503 (2008). . M. Alvioli, C. Ciofi degli Atti, L. P. Kaptari, C. B. Mezzetti, H. Morita and S. Scopetta, Phys. Rev. C **85**, 021001 (2012)
- [20] R. B. Wiringa, V. G. J. Stoks and R. Schiavilla, Phys. Rev. C**51**, 38 (1995).
- [21] A. Kievsky, S. Rosati and M. Viviani, Nucl. Phys. A **551**, 241 (1993).
- [22] H. Kamada, *et al*, Phys. Rev. C**64**, 044001 (2001).
- [23] R. Jastrow, Phys. Rev. **98**, 1479 (1955).
- [24] R. Schiavilla, R. B. Wiringa, S. C. Pieper and J. Carlson, Phys. Rev. Lett. **98**, 132501 (2007).
- R. B. Wiringa, R. Schiavilla, S. C. Pieper and J. Carlson, Phys. Rev. C **89**, 024305 (2014).
- [25] S. C. Pieper, R. B. Wiringa, V. R. Pandharipande, Phys. Rev. C**46**, 1741(1992)
- [26] D. Lonardoni, A. Lovato, S. C. Pieper, R. B. Wiringa, arXiv:1705.04337v1 [nucl-th]
- [27] E. Feenberg, *Theory of quantum fluids*, Academic press, New York and London, 1969.
- [28] S. Fantoni, S. Rosati, Nuovo Cimento A**43**, 413 (1978).
- [29] F. Arias de Saavedra, C. Bisconti, G. Co' and A. Fabrocini, Phys. Rept. **450**, 1 (2007)
- [30] J. W. Clark, Progr. Part. Nucl. Phys. **2**, 89 (1979).
- [31] M. Gaudin, J. Gillespie and G. Ripka, Nucl. Phys. A**176**, 237 (1971).
- [32] O. Bohigas and S. Stringari, Phys. Lett. B**95**, 9 (1980).
- [33] M. Alvioli, C. Ciofi degli Atti, H. Morita, Phys. Rev. C**72**, 054310 (2005).
- M. Alvioli, C. Ciofi degli Atti, L. P. Kaptari, C. B. Mezzetti, H. Morita Phys. Rev. C **87**, 034603 (2013)
- [34] J. Ivon, Act. Sci. Ind. **203** (1965).
- J. E. Mayer and M. G. Mayer, Statistical Mechanics, Wiley, New York and London, 1940.
- [35] C. Ciofi degli Atti, C. B. Mezzetti, H. Morita, Phys. Rev. C**95**, 044327 (2017).
- [36] O. Arviles, M. Sargsian, Phys. Rev. C**94**, 064318 (2016). .

TABLE I: A comparison of the results of three-realistic many-body calculations for the ground-state energy and r.m.s. radius of $A = 16$ obtained by the minimization of Eq. (25): Cluster Variational Monte Carlo (CVMC) [26], Normalization Conserving Linked Cluster Expansion (NCLCE) [33]. The three methods are variational ones and use Woods-Saxon single-particle wave functions and similar 2N interactions, with and without 3N UIX interaction. Energies in MeV and radii in fm .

Mean Field	Approach	Potential	(E/A)	$(E/A)_{exp}$	$\langle r^2 \rangle^{1/2}$	$(\langle r^2 \rangle^{1/2})_{exp}$
WS	NCLCE	AV8'	-4.4	-7.98	2.64	2.69
WS	CVMC	AV18	-5.5	-7.98	2.54	2.69
WS	CVMC	AV18+UIX	-5.15	-7.98	2.74	2.69

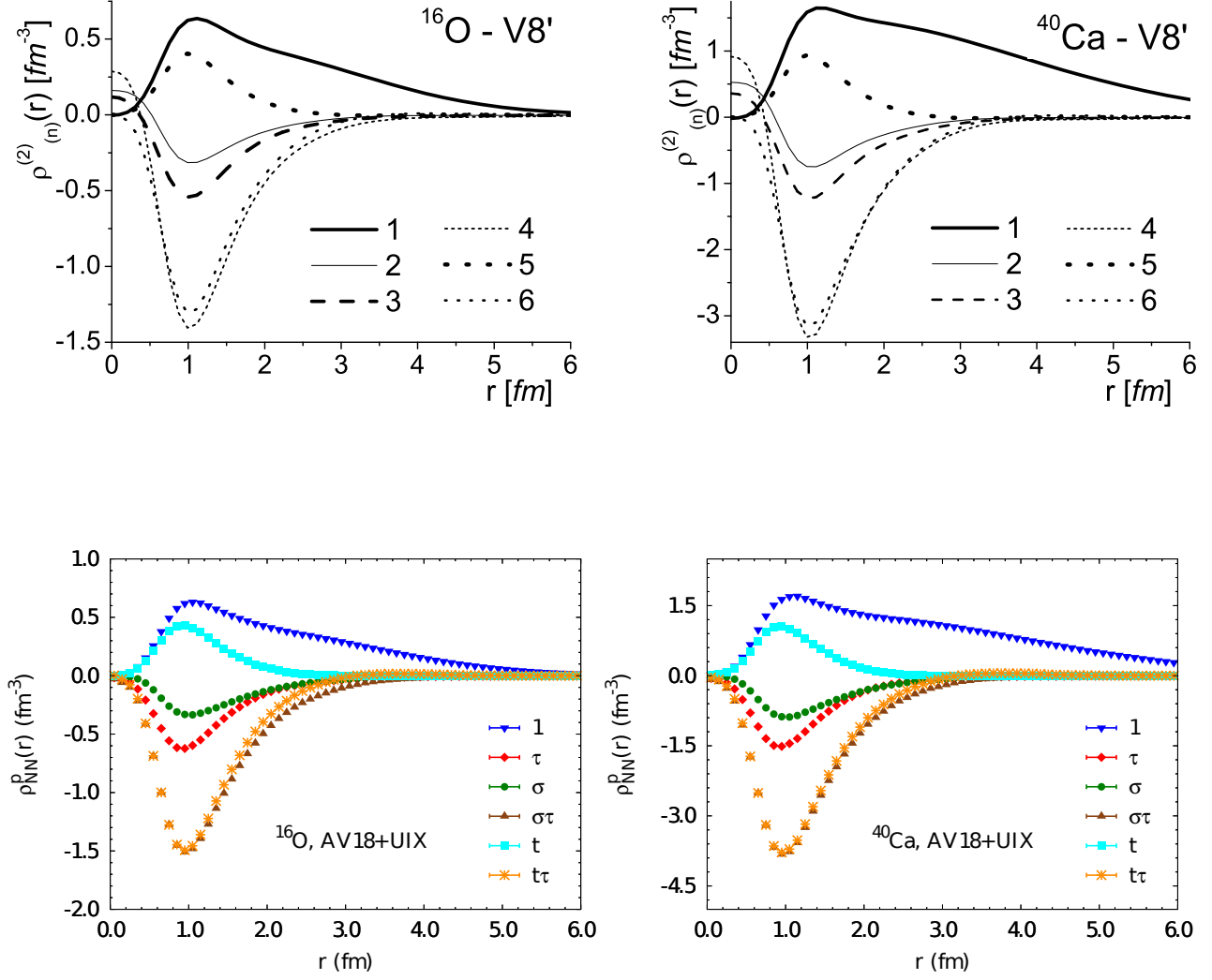


FIG. 1: **Upper panel:** the two-body density $\rho_n^{(2)}(r = |\mathbf{r}_1 - \mathbf{r}_2|)$ obtained in the variational NCLCE calculation of Ref. [33] performed with the first six components of the Argonne $V8'$ NN interaction (Eq. (24)) corresponding to the values of the ground-state energy and radius listed in Table I. **Lower panel:** the same as in the upper panel but in the case of the calculation of Ref. [26] performed with the $AV18$ NN interaction plus UIX $3N$ interaction.

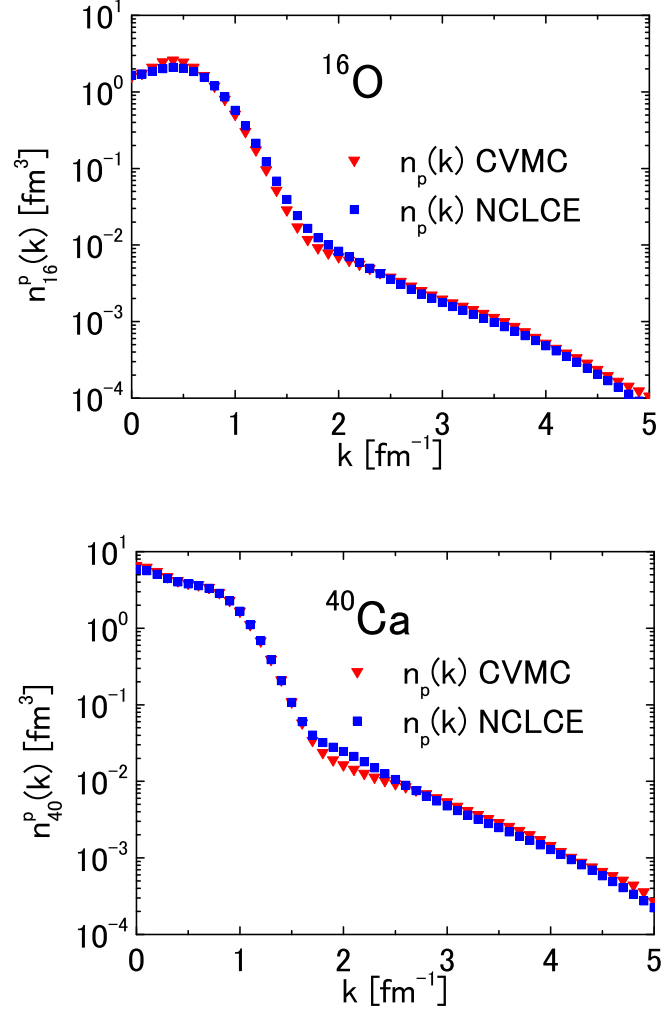


FIG. 2: The proton ($n_p = n_n$) one-nucleon momentum distribution of ^4He and ^{16}O obtained in Ref. [26] within the Cluster Variational Monte Carlo (CVMC) and in Ref. [33] within the NCLCE at the lowest order.

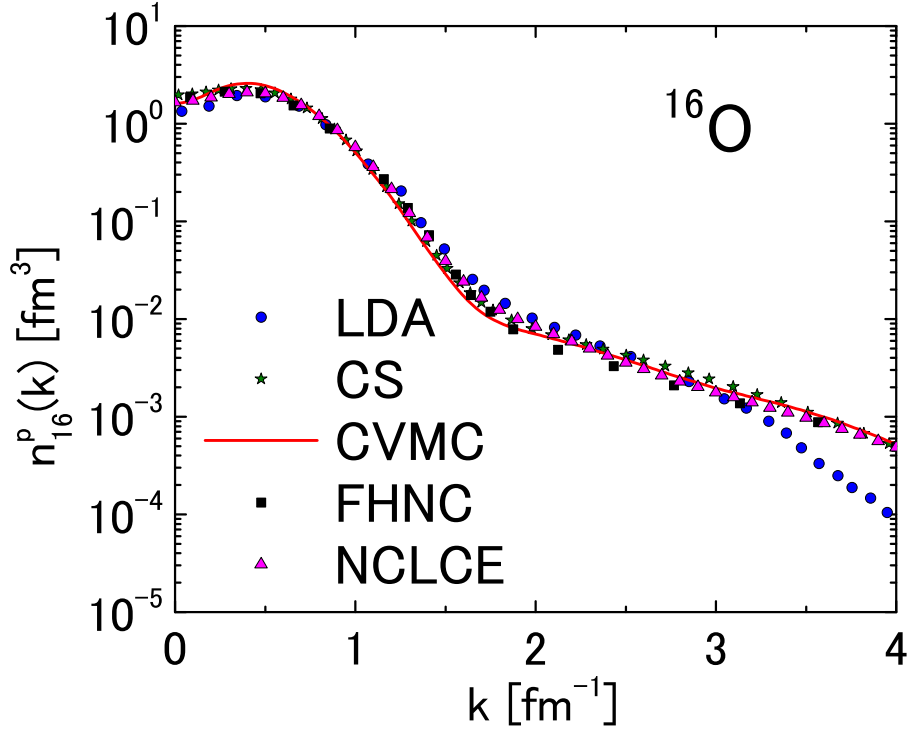


FIG. 3: (Color online) The momentum distributions of ^{16}O calculated with different many-body approaches and similar realistic NN interactions: the Cluster Variational Monte Carlo (CVMC) results of Ref. [26] (full line); the Normalization Conserving Linked Cluster Expansion (NCLCE) Ref. [33] (triangles); the Fermion Hypernetted Chain Method (FHNC) of Ref. [29] with V8' interaction (squares); the two-nucleon correlation model (CS) of Ref. [8] (asterisks); the full dots represent the momentum distributions obtained by integrating the SF obtained within the nuclear matter Local Density Approximation (LDA) [6, 9].

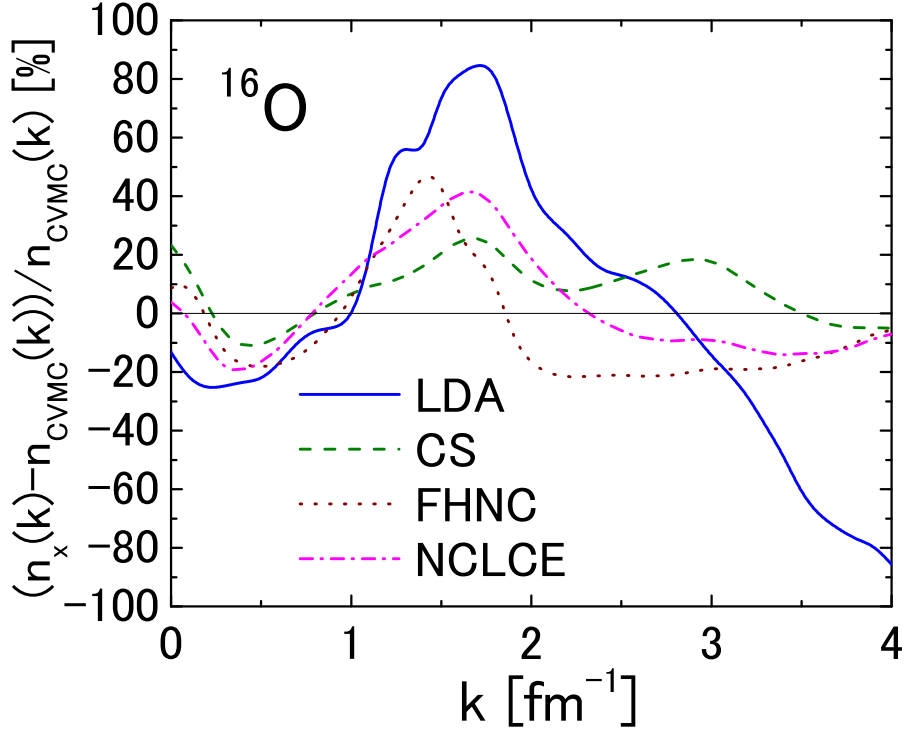


FIG. 4: (Color online) The quantity $100 \frac{\Delta n(k)}{n_{VMCV}}$ (Eq. (37)) i.e. the percent deviation of the microscopic calculations of the momentum distributions of ^{16}O shown in Fig. 3 taking the CVMC results of Ref. [26] as the reference results. LDA: Ref. [6, 9]; CS: Ref. [8]; FHNC: Ref. [29]; NCLCE: Ref. [33].

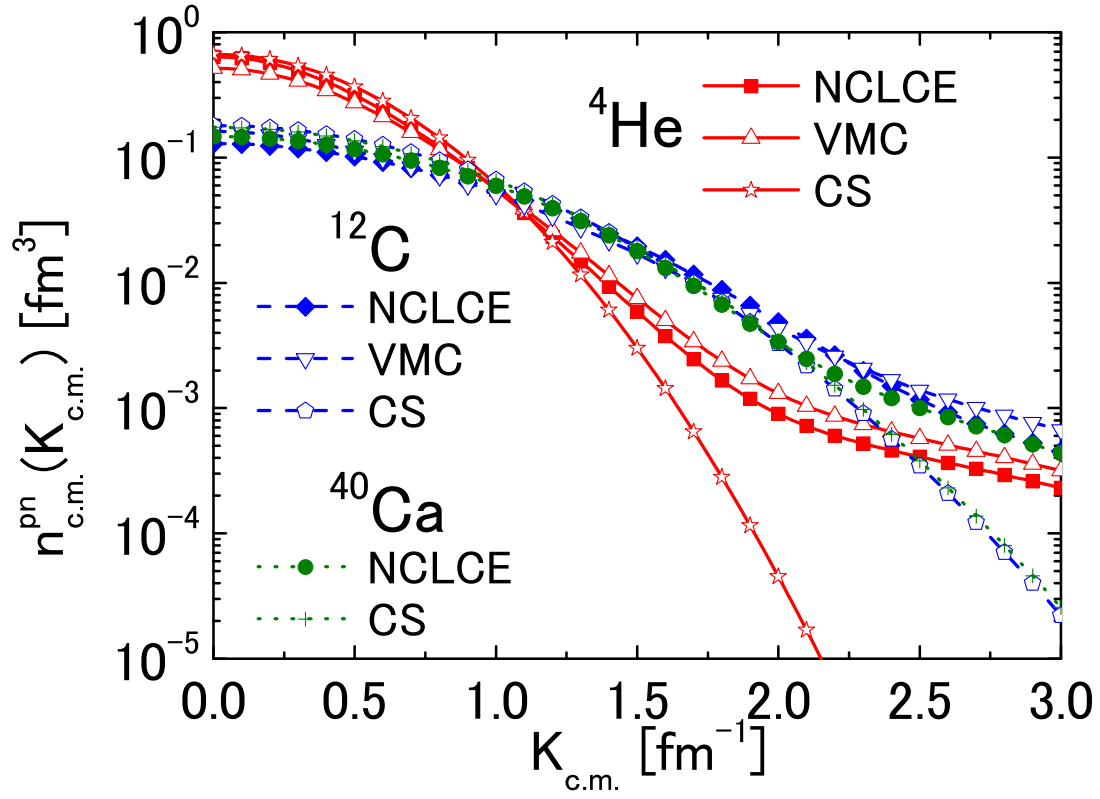


FIG. 5: (Color online) The proton-neutron center-of-mass (c.m.) momentum distributions (Eq. (39)) in ^4He , ^{12}C and ^{40}Ca calculated within microscopic many-body approaches. NCLCE: Ref. [19]; VMC: Ref. [24]; CS: Ref. [8].

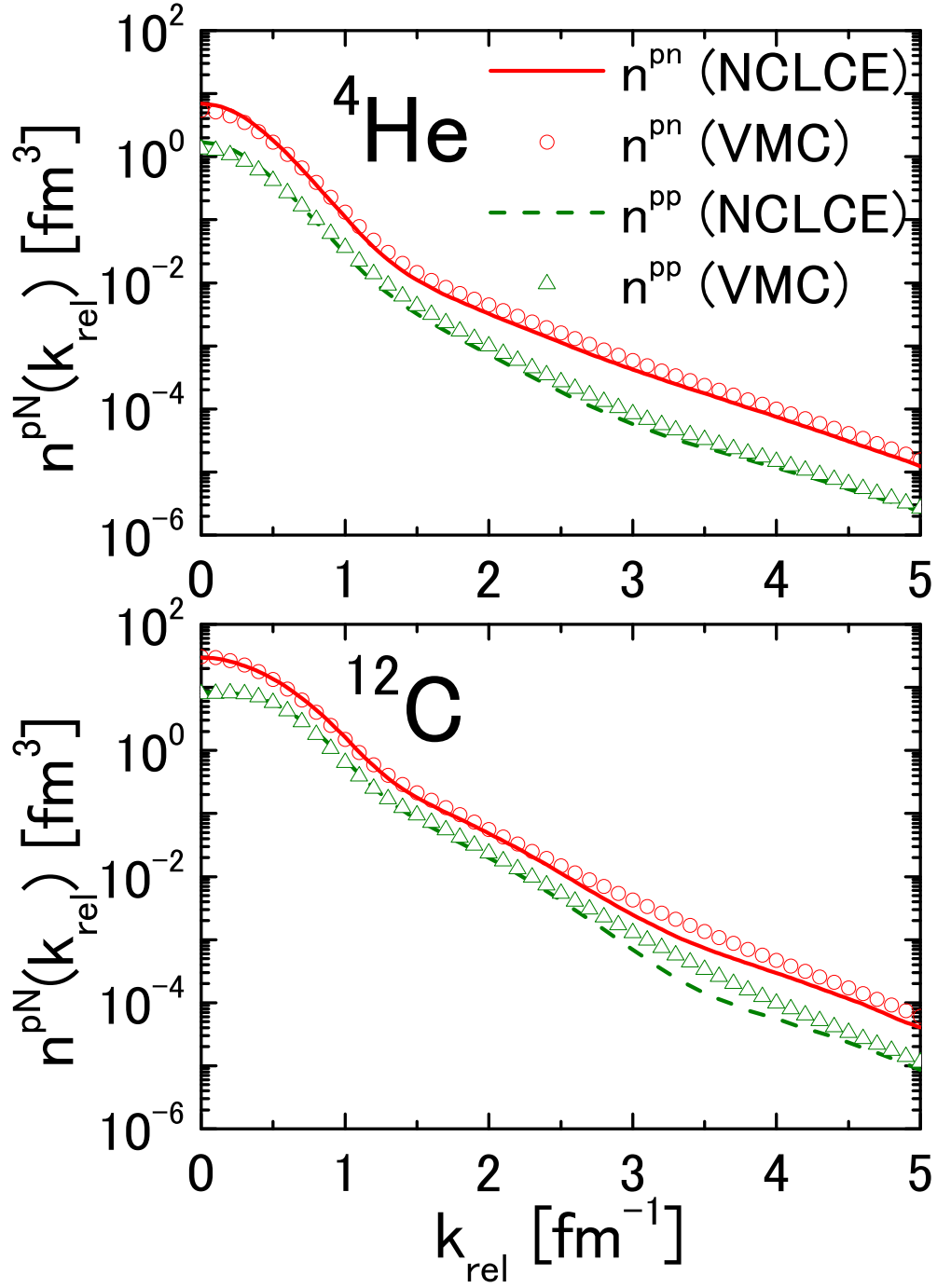


FIG. 6: (Color online) The pn and pp relative momentum distributions (Eq. (40)) in ${}^4\text{He}$ and ${}^{12}\text{C}$ calculated by the NCLCE (lines) [19] and the VMC (symbols) [24].

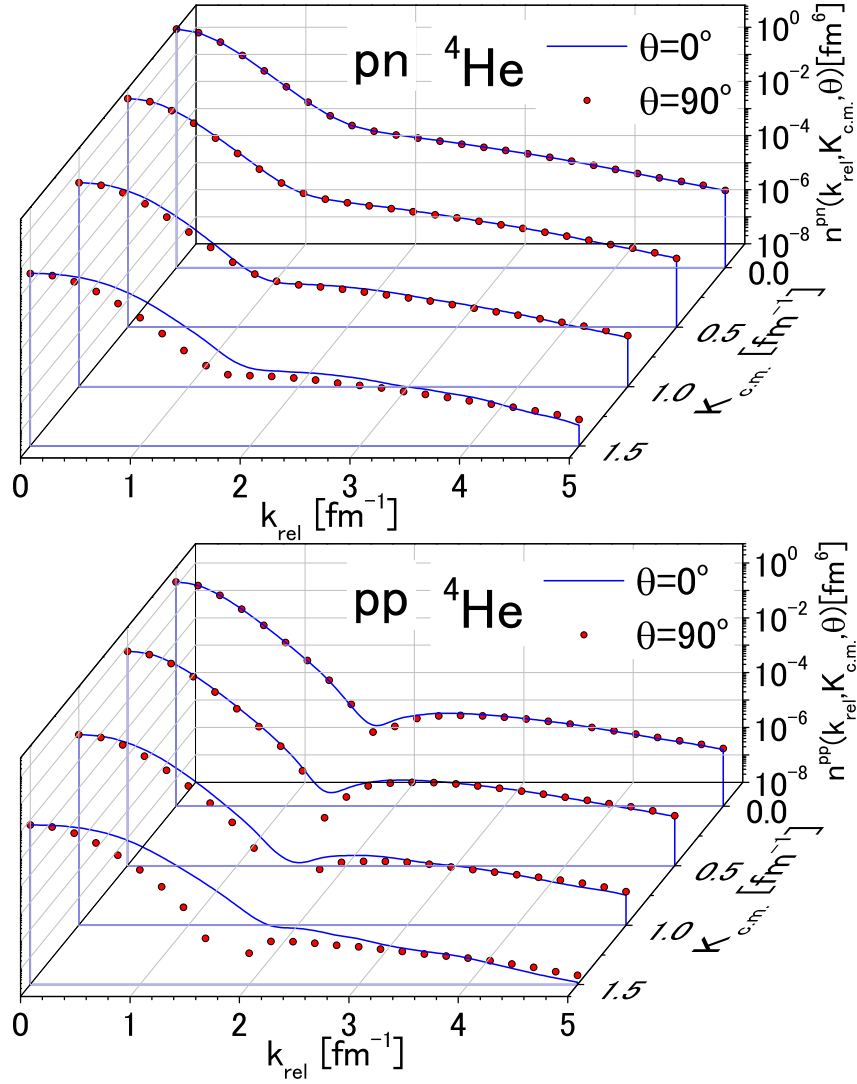


FIG. 7: (Color online) The pn and pp two-nucleon momentum distributions in ${}^4\text{He}$, $n^{pn}(k_{rel}, K_{c.m.}, \theta)$, obtained in Ref. [19] in correspondence of several values of $K_{c.m.}$ and two values of the angle θ between $\mathbf{K}_{c.m.}$ and \mathbf{k}_{rel} . The region of k_{rel} where the value of $n^{pn}(k_{rel}, K_{c.m.}, \theta)$ is independent of the angle determines the region of factorization of the momentum distributions, i.e. $n^{pn}(k_{rel}, K_{c.m.}, \theta) \rightarrow n_{rel}^{pn}(k_{rel})n_{c.m.}^{pn}(K_{c.m.})$. It can be seen that the region of factorization starts at values of $k_{rel} = k_{rel}^-$, which increases with increasing values of $K_{c.m.}$, i.e. $k_{rel}^- = k_{rel}^-(K_{c.m.})$; because of the dependence of k_{rel}^- upon $K_{c.m.}$, a constraint on the region of integration over $K_{c.m.}$ arises from Eq. (43).

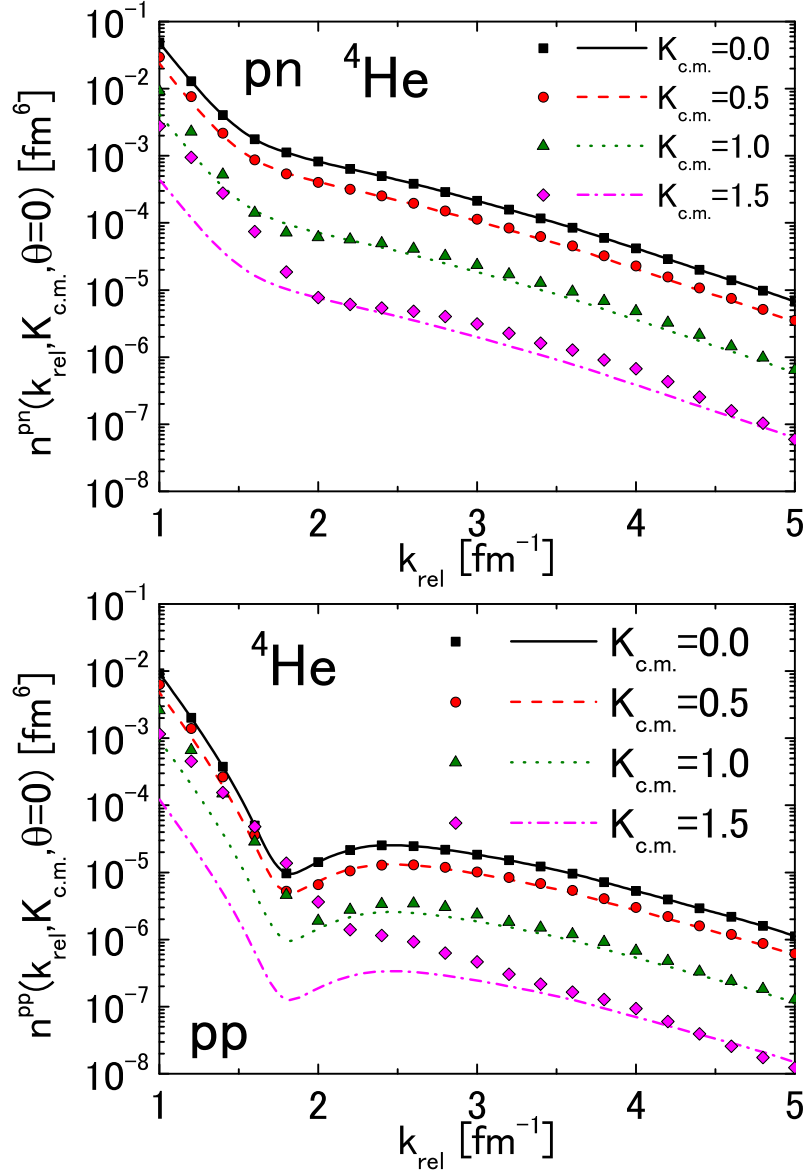


FIG. 8: (Color online) The pn and pp two-nucleon momentum distributions $n^{pN}(k_{rel}, K_{c.m.}, \theta = 0)$ for ${}^4\text{He}$ (symbols) compared with the results of Eq. (44) (lines), where for pn and pp Eq. (45) and Eq.(48), respectively have been used.

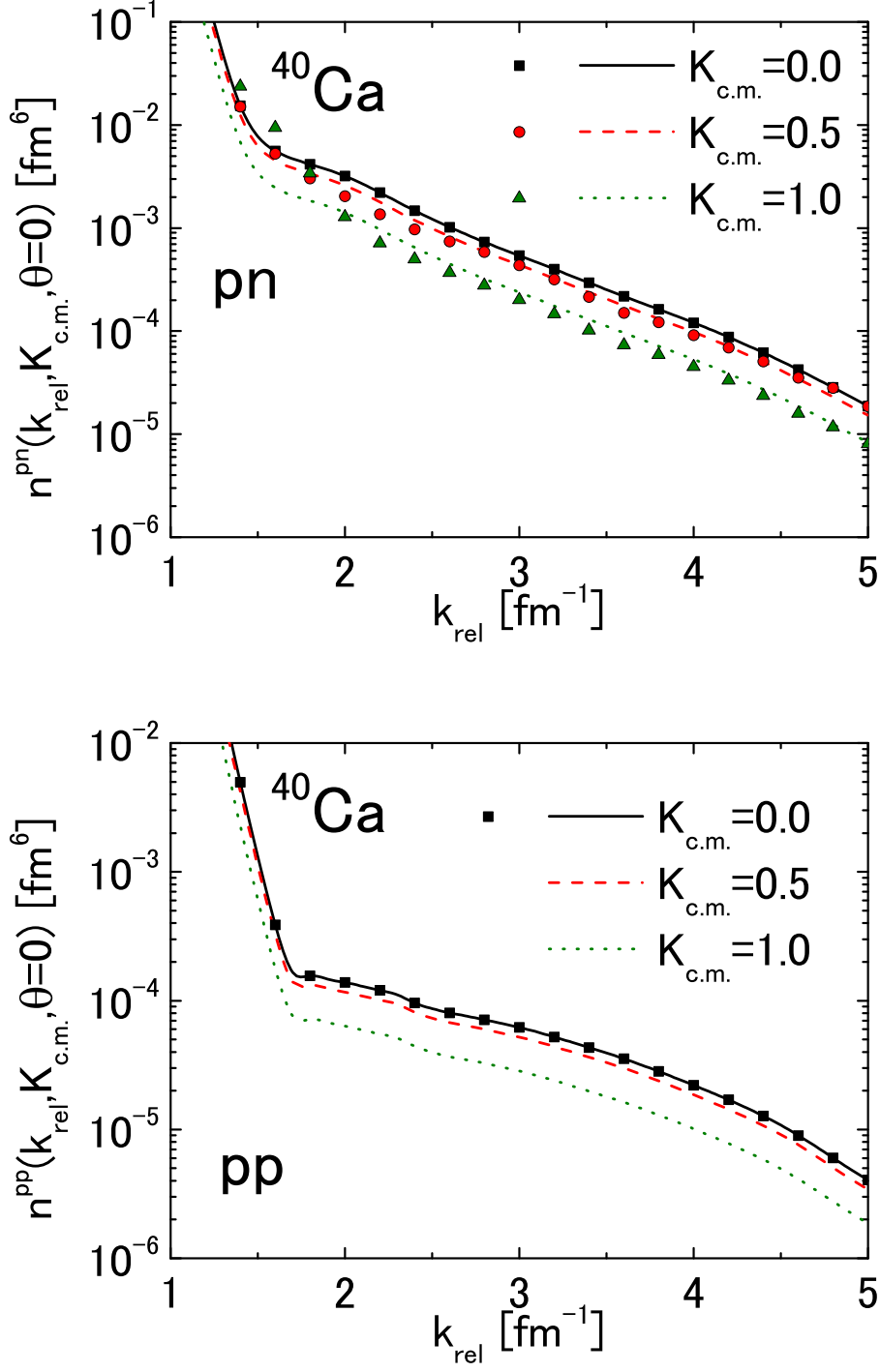


FIG. 9: (Color online) The same as in Fig. 8 but for ^{40}Ca .

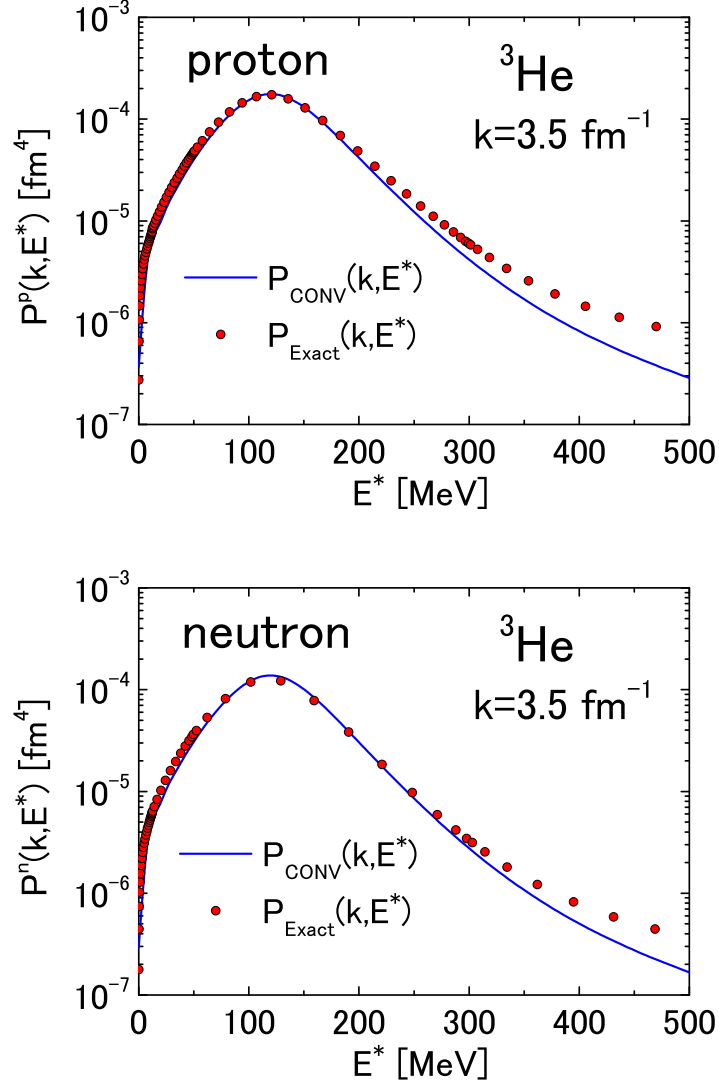


FIG. 10: (Color online) The *ab-initio* proton and neutron SF of ^3He from Ref. [3] (red dots) compared with the convolution SF (Eq. (50), full line) obtained taking into account the constraint (Eq. (43)) on the value of k_{rel}^- which guaranties that the convolution formula includes indeed only the factorization region

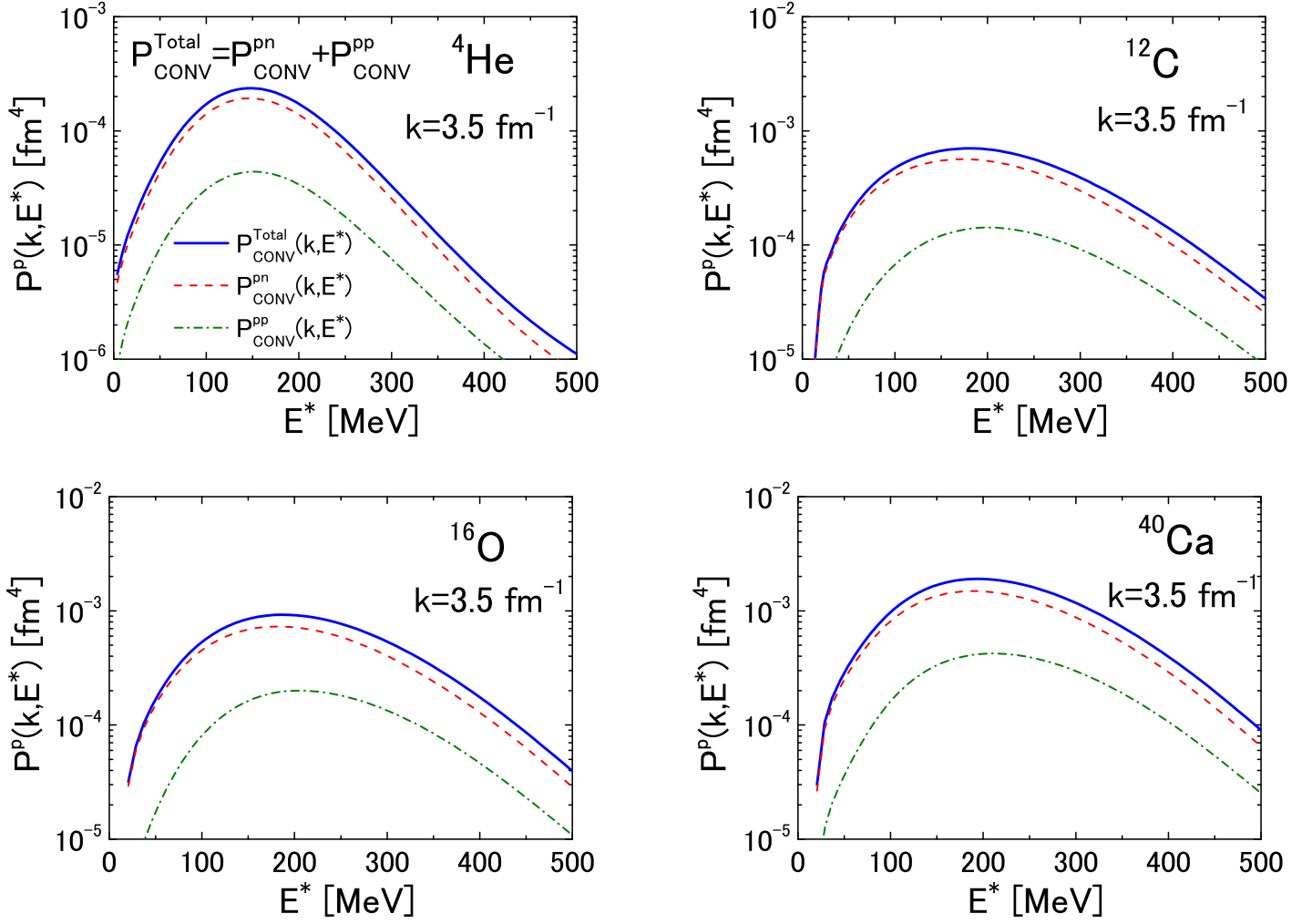


FIG. 11: (Color online) The SF of ${}^4\text{He}$, ${}^{12}\text{C}$, ${}^{16}\text{O}$, and ${}^{40}\text{Ca}$ calculated with the convolution SF (Eq. (50)). The dashed and dot-dashed lines represent, respectively, the pn and the pp SRC contributions.

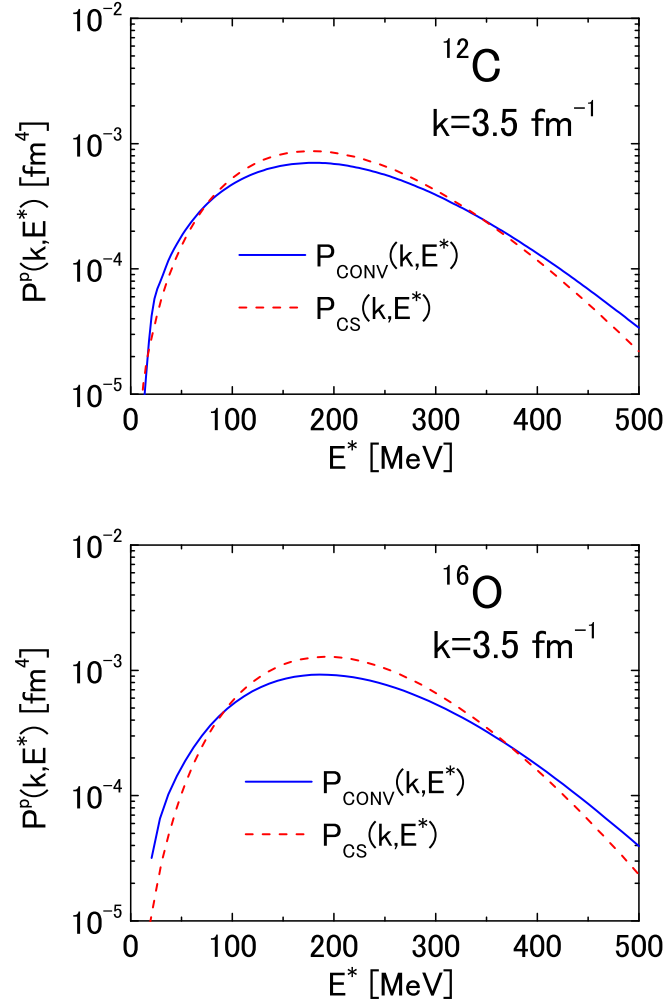


FIG. 12: (Color online) The convolution spectral of ^{12}C (Eq. (50)) and ^{16}O (full line) compared with the effective convolution formula from Ref. [8] (dashed line).

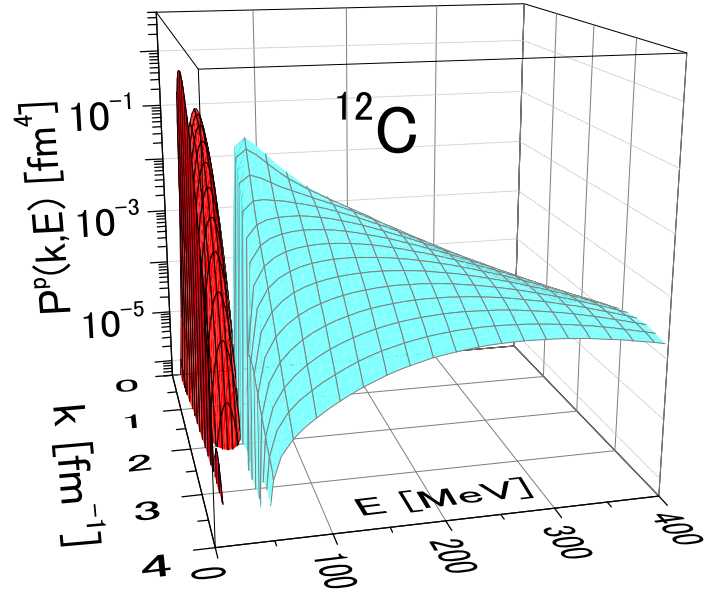


FIG. 13: (Color online) A 3D figure of the total SF (Eq. (49)) of ^{12}C illustrating the mean-field and SRC contributions: $P_{MF}^{N_1}(k, E)$ (shown in Red) is located in the region of removal energy $E \leq 50 \text{ MeV}$ where the contribution from the $\ell = 1$ and $\ell = 0$ shells can be identified, whereas $P_{SRC}^{N_1}(k, E)$ (shown in Blue) completely exhausts the removal energy region with $E \geq 50 \text{ MeV}$.

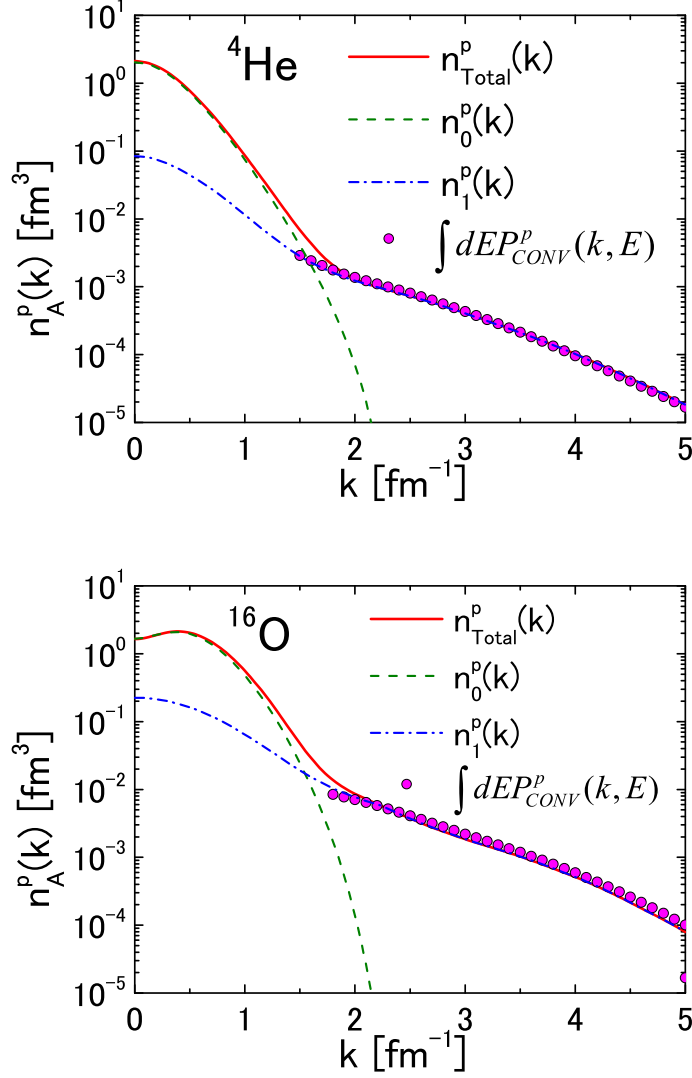


FIG. 14: (Color online) *The SRC Momentum sum rule $n_{SRC}(k) \equiv n_1(k) = \int_0^\infty P(k, E^*) dE^*$ in ^4He and ^{16}O . The full line represents the total momentum distribution obtained in Ref. [33] with the dashed and dot-dashed curves corresponding to the mean-field and SRC contributions, respectively. The full dots represent the the SRC momentum distribution obtained by integrating the the SRC convolution SF. It can be seen that the momentum sum rule is exactly satisfied by the convolution formula.*

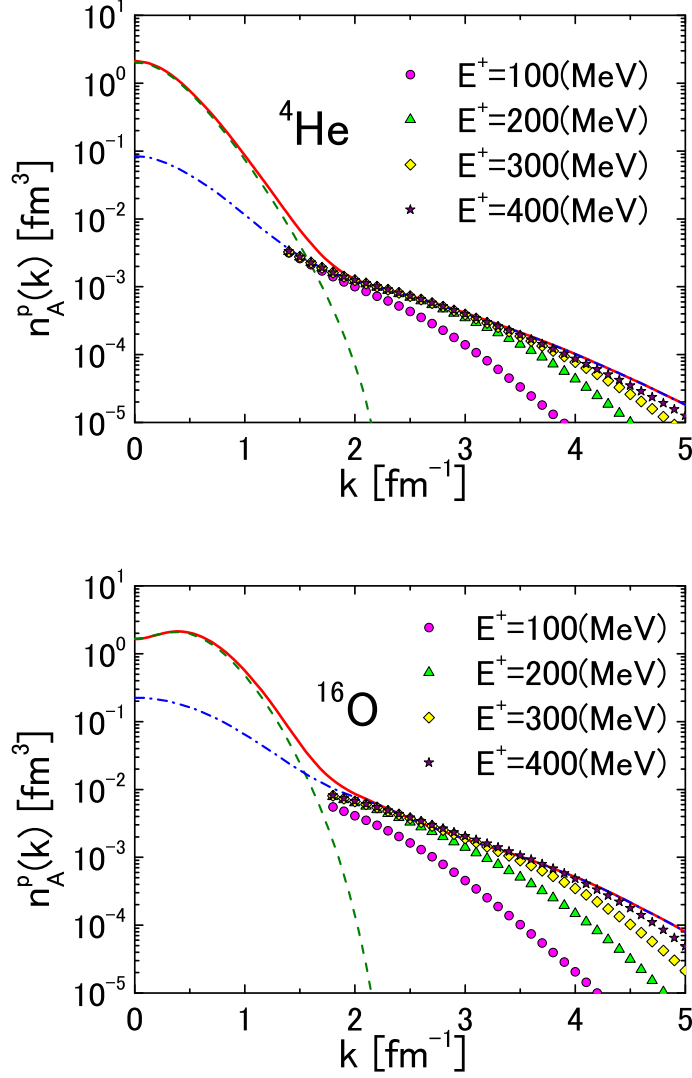


FIG. 15: (Color online) *The convergence of the momentum sum rule $n_{SRC}(k) \equiv n_1(k) = \int_0^{E^+} P(k, E^*) dE^*$. The partial momentum sum rule corresponding to increasing value of E^+ . It can be seen that in order to obtain the correct momentum distributions in the region $k \geq 4 \text{ fm}^{-1}$ it is necessary to integrate the SF up to $E^+ \simeq 400 \text{ MeV}$. Full, dashed and dot-dashed curves as in Fig. 14.*